Pilus production in *Acinetobacter baumannii* is growth phase dependent and essential for natural transformation

Nina Vesel and Melanie Blokesch*

Laboratory of Molecular Microbiology, Global Health Institute, School of Life Sciences, Ecole Polytechnique Fédérale de Lausanne (EPFL), CH-1015 Lausanne, Switzerland.

* Correspondence: melanie.blokesch@epfl.ch

Keywords: *Acinetobacter baumannii*; natural competence for transformation; type IV pili; twitching motility

Running title: Transformation and pili in *A. baumannii*

ABSTRACT

Acinetobacter baumannii is a severe threat to human health as a frequently multidrug-resistant hospital-acquired pathogen. Part of the danger from this bacterium comes from its genome plasticity and ability to evolve quickly by taking up and recombining external DNA into its own genome in a process called natural competence for transformation. This mode of horizontal gene transfer is one of the major ways pathogens can acquire new antimicrobial resistances and toxic traits. Because these processes in *A. baumannii* are not well studied, we herein characterized new aspects of natural transformability in this species that include the species' competence window. We uncovered a strong correlation with a growth–phase-dependent synthesis of a type IV pilus (TFP), which constitutes the central part of competence-induced DNA-uptake machinery. We used

bacterial genetics and microscopy to demonstrate that the TFP is essential for the natural transformability and surface motility of *A. baumannii*, whereas pilus-unrelated proteins of the DNA-uptake complex do not impact the motility phenotype. Furthermore, TFP biogenesis and assembly is subject to input from two regulatory systems that are homologous to *Pseudomonas aeruginosa*, namely the PilSR two-component system and the Pil-Chp chemosensory system. We demonstrated that these systems not only impact the piliation status of cells but also their ability to take up DNA for transformation. Importantly, we report on discrepancies between TFP biogenesis and natural transformability within the same genus by comparing *A. baumannii* to data reported for *A. baylyi,* the latter of which served for decades as a model for natural competence.

IMPORTANCE

Rapid bacterial evolution has alarming negative impacts on animal and human health, which can occur when pathogens acquire antimicrobial resistance traits. As a major cause of antibiotic-resistant opportunistic infections, *A. baumannii* is a high priority health threat, which has motivated renewed interest in studying how this pathogen acquires new, dangerous traits. In this study, we deciphered a specific time window in which these bacteria can acquire new DNA, and correlated that with its ability to produce the external appendages that contribute to the DNA acquisition process. These cell appendages function doubly for motility on surfaces and for DNA uptake. Collectively, we showed that *A. baumannii* is similar in its TFP production to *Pseudomonas aeruginosa*, though differs from the well-studied species *A. baylyi*. This discovery is key, as assumptions about the behavior of the less-studied *A. baumannii* are often erroneously taken from that of *A. baylyi*. This knowledge will guide future endeavors to better understand HGT and antimicrobial resistance in hospital pathogens such as *A. baumannii*.

45

46 **INTRODUCTION**

47 Bacterial evolution is a major human health concern, as it can lead to the acquisition of concerning
48 traits, such as new antimicrobial resistances or virulence genes. One pathogen of concern is the
49 hospital-prevalent antimicrobial-resistant *Acinetobacter baumannii* (1, 2), which evolves rapidly
50 by incorporating significant amounts of DNA from other organisms in a process called horizontal
51 gene transfer (HGT) (3). Using a type of HGT called natural competence for transformation, *A.*
52 *baumannii* is able to take up extracellular DNA from its environment and incorporate it into its
53 own genome by homologous recombination (4-7). We recently reported that such transformation
54 events can lead to frequent exchanges of genomic regions greater than 100 kbp in the naturally
55 competent bacterium *Vibrio cholerae*, which could explain how bacteria such as *A. baumannii*
56 acquire new DNA stretches including resistances. However, few reports have addressed natural
57 competence in *A. baumannii*, instead extrapolating its behavior based off that of the soil bacterium
58 *A. baylyi* (8, 9).

59 The few studies on transformation in *A. baumannii* have focused mainly on mild competence
60 inducers such as serum albumin and Ca^{2+}, on transforming materials, and the pH (10-12).
61 However, transforming protocols vary wildly between studies (13-15), including the use of
62 different solidifying agents for transformation scoring on surfaces (16). Additionally, only few
63 isolates of this species, such as the strains A118 (13) and M2 (recently reclassified as *A.*
64 *nosocomialis*) (15, 17), were previously found to be naturally competent, though recent studies are
65 showing that a plethora of clinical and wildlife/livestock *A. baumannii* isolates are likewise
66 naturally transformable (12, 14, 18). Therefore, the process of natural competence in *A. baumannii*
67 needs to be better studied and recorded.

Additionally, a number of studies have shown the inducement of transformation potential in a surface-dependent manner, suggesting a correlation between natural transformability and the movement of *A. baumannii* on (wet) surfaces (14, 15). This correlation is thought to be based on the bacterium's ability to produce type IV pili (TFP) (15), which are cell appendages that frequently constitute the central part of the DNA-uptake machinery (7) (Fig. 1A). Known to play a main role in the DNA-uptake complex, the regulation of TFP production is often linked to the bacterium's competence program (6). For instance, in *V. cholerae*, the TFP, which enhances the bacterium's natural transformability, is only produced when the bacterium grows on chitinous surfaces (19-23). Considering that TFP also mediate other functions that include adhesion, motility on surfaces (i.e., twitching motility), and surface sensing (24), it makes sense that the TFP would be the link between transformability and mobility in *A. baumannii*.

To better understand these dual roles of this dynamic TFP, it is important to understand when it is produced in the bacterium. The TFP is composed of major (PilA) and minor pilin subunits (different kinds in diverse bacteria), and extension and retraction events are energized by the cytosolic PilB and PilT/PilU ATPases, respectively. Upon or after TFP retraction, the incoming transforming DNA enters the periplasmic space through the PilQ secretin where it is bound by the DNA-binding protein ComEA. This protein is thought to act as a Brownian ratchet, which leads to the accumulation of long stretches of DNA within the bacterium's periplasm (21, 25). After degradation of one strand, which, in Gram-negative bacteria, is attributed to an unidentified nuclease or a periplasmic extension of the ComEC protein, the single-stranded DNA translocates across the inner membrane through the ComEC channel aided by the ComF protein (Fig. 1A). Once in the cytosol, the single-stranded DNA is bound by the single-stranded binding protein Ssb, the RecA-loading protein DprA, and RecA. RecA ultimately fosters recombination if the

transforming DNA is homologous with the chromosomal DNA of the cell. ComM (a RadA homolog) assists in this process, especially if heterologous DNA is present between the homologous flanks (26, 27).

There are different types of TFP regulatory systems, which exist in both competent and non-competent bacteria. A major TFP regulatory system that has been studied in *Pseudomonas aeruginosa* (a bacterium that was only recently reclassified as naturally transformable; (28)) is the two-component system (TCS) PilSR (29-31). The current model of this TCS suggests that extended pili are sensed due to the lack of inner membrane-associated PilA subunits that would otherwise interact with the atypical sensor histidine kinase PilS. The lack of interaction stimulates PilS's kinase activity, which leads to activation of the response regulator PilR and, ultimately, *pilA* transcription (32). This PilS-mediated pilin inventory and its impact on PilR activity also influence other co-regulated processes involved in virulence and surface-associated bacterial behavior (33). The Pil-Chp chemosensory system also plays a role in TFP assembly and twitching motility (34, 35). This system is composed of ten or more components, which are mostly encoded by the *pil-chp* operon (*pilGHIJK-chpABC*) in *P. aeruginosa* (36, 37), and was shown to react to mechanosensing signals upon surface attachment (38). The main components of the system are a transmembrane chemoreceptor (PilJ), a histidine kinase (ChpA), and the response regulators PilG and PilH, all of which share homology with flagellar chemotaxis proteins (39). The response regulators modulate intracellular cAMP levels by regulating the activity of the adenylate cyclase CyaB (40, 41). Increased intracellular cAMP levels subsequently activate the virulence regulator Vfr (42). Importantly, PilG and PilH also regulate TFP dynamics in a cAMP-independent manner by modulating PilB-driven pilus extension and PilT-driven pilus retraction, respectively (36, 40).

In this study, we characterized aspects of the natural competence program of *A. baumannii*. We showed that the pathogen's transformability varies significantly during the different growth phases. This variability is due to growth phase-dependent production of its TFP. From genetically engineered mutants and pilus visualization, we demonstrated that pilus-related genes are essential for the bacterium's transformability and its surface motility, while pilus-unrelated competence genes do not interfere with the motility phenotype. Based on their homology to their *P. aeruginosa* counterparts, we identified several conserved TFP regulators and showed that these regulators impact cellular piliation status and influence natural transformation in *A. baumannii*.

RESULTS AND DISCUSSION

Transformation of *A. baumannii* occurs mostly during exponential growth

To begin, we sought the optimized conditions for transformability for strain A118 (13)(Table 1) by adapting variations from different available protocols. We found the ideal conditions to be after aerobic growth in broth followed by DNA uptake on agar surfaces (see methods). We next tested the impact of the growth phase during the liquid culturing time on the bacterial transformability. As shown in Figure 1B, the highest levels of transformation were observed for bacteria grown to the exponential phase (i.e., ~90 min), while the strain's transformability fell below detection after *A. baumannii*'s dilution into fresh medium or upon entry into the stationary phase (Fig. 1). This behavior is distinct from *A. baylyi,* which can reach transformation frequencies up to 0.7% of all cells (43) and is transformable throughout all growth phases with varying efficiencies (44, 45). This underscores the importance of studying *A. baumannii* in its own right and not relying on assumptions made from model bacteria.

135 To better understand this rather tight transformation window, we scored transcript levels of
136 selected competence genes as a function of time. To identify competence genes in *A. baumannii*
137 A118, we investigated its previously published genome sequence, where Ramirez *et al.* reported
138 186 scaffolds at least 500 bp in length (46). However, the overall high number of contigs (1647
139 contigs, accession number AEOW01000000) complicated the search for genes and the
140 determination of operons. Therefore, we re-sequenced the strain using long-read PacBio
141 technology and *de novo* assembled its genome (see methods).

142 With the 3,750,370 bp closed genome of *A. baumannii* at hand (Table 2), we then identified all
143 known competence genes based on homology to the competent model organisms *A. baylyi* and *V.*
144 *cholerae* (20, 47) (Table 3). Next, we scored the transcript levels of six selected competence genes:
145 *pilA, pilQ, pilT*, *comEA*, *comEC*, and *dprA.* The encoded products of these genes (e.g., the major
146 pilin subunit PilA, the outer membrane secretin PilQ, and the retraction ATPase PilT) contribute
147 to the assembly of the central TFP of the DNA uptake machinery and are key for DNA uptake in
148 Gram-negative bacteria. They are also important for DNA translocation across the outer (ComEA)
149 and inner (ComEC) membrane or in recombination-mediating activity (DprA) inside the cytosol
150 (7) (Fig. 1A). As shown in Figure 1C, the transcript levels varied at time points before, during, and
151 after the growth phase in which transformation levels were the highest (Fig. 1B). In general, the
152 *pil* genes specifically peaked around 90 min after dilution (Fig. 1C), which correlated with the
153 beginning of the transformation window (Fig. 1B). This differed from previous reports on *A. baylyi*
154 where Porstendörfer *et al*. showed that the expression of the *pilA* homologues major pilin gene
155 *comP* decreased immediately after dilution into fresh medium, with the lowest levels in the mid-
156 exponential phase. In their study, maximal *comP* expression levels were observed in the late
157 stationary phase (45).

158 **Peak transformation coincides with type IV pilin production**

159 As transcript levels do not necessarily reflect the cellular protein levels, we next tested the
160 production of the major pilin protein PilA. To accomplish this, we translationally fused PilA to a
161 short FLAG-tag, which gave a strain with the *pilA-FLAG* allele at the native *pilA* locus that retained
162 suboptimal but still high transformation levels (Fig. 1D). We grew this genetically engineered
163 strain and quantified the PilA-FLAG protein levels in cells over time by Western blotting. From
164 these data, we concluded that no PilA-FLAG was detected early on in growth. We observed that
165 the major pilin level peaked at approximately 90 to 105 min post-dilution (OD_{600} of ~0.6–0.7),
166 declined after 120 min of growth (OD_{600} of ~1.0), and ultimately disappeared later in the growth
167 phase (Fig. 1E). To control for surface-exposed pili that might have been lost through shearing
168 during the harvesting process, we repeated the same experiment in a *pilQ*-deletion strain in which
169 pili cannot cross the outer membrane. We observed a similar protein production pattern over time
170 (Fig. 1F) to that of the parental wildtype (WT) background strain (Fig. 1E). From these data, we
171 concluded that *A. baumannii* produces its TFP solely during the early exponential phase under
172 liquid growth conditions. This is in stark contrast to *A. baylyi* in which the major pilin is primarily
173 produced in the stationary phase and is either absent or only present at low levels during the
174 exponential growth phase (45).

175

176 **Pilus visualization elucidates diverse phenotypes**

177 We extended our study beyond quantification of the major pilin subunit by visualizing the TFP of
178 *A. baumannii.* To do so, we aimed at using thiol-reactive maleimide-conjugated dyes to cysteine-
179 containing cell appendages, an approach that has been used for the flagellum of *Bacillus subtilis*
180 (48) and the tight adherence (Tad) pilus of *Caulobacter crescentus* (49). To determine the proper

location for a site-directed cysteine knock-in into the major pilin PilA, we followed the same protocol as described for *V. cholerae* (22). Briefly, we predicted the surface-exposed αβ-loop of PilA using the Phyre2 web portal (50) (Fig. 2A) and found that the overall structure prediction for *A. baumannii*'s PilA was similar to that of *V. cholerae* (Fig. 2A) by length and homology in the protein's N-terminal region. From this analysis, we selected an alanine-to-cysteine mutation at position 61 (A61C), which is comparable to the cysteine knock-in mutant we had previously determined for *V. cholerae* (PilA[S67C]; (22, 51)). We tested the transformation efficiency of the new A118-PilA[A61C] strain relative to the parental WT strain. As shown in Figure 2B, the strain's transformation efficiency was reduced by approximately 18-fold compared to the WT, but it nonetheless maintained robust transformability. To potentially improve the transformation efficiency of cysteine knock-in mutants, we next designed and tested six additional site-directed mutants with amino acid exchanges in the predicted surface-exposed region ([G60C], [V62C], [T64C], [T72C], [T75C], [S77C]). None of these variants resulted in significantly higher transformation levels compared to the strain producing PilA[A61C] (Fig. 2B). Therefore, we proceeded with the PilA[A61C] strain given that our previous work on *V. cholerae* had identified this region as appropriate for the pilus labeling process (22).

To visualize the cells' pili, we next grew the PilA[A61C] strain to an optical density of ~0.6–0.7, as pilin levels were highest at this growth stage (Fig. 1E). At this time point, we added the thiol-reactive dye (Alexa Fluor 488 C_5 maleimide) to the culture, then incubated, washed, and mounted the bacteria onto agarose pads. As shown in Figure 2C, the bacteria produced pili that, for some cells, extended far beyond the outer membrane. Notably, such extended pili were not restricted to one side of the cell body as recently described for *A. baylyi* in a preprinted study (52). The bodies of the cells were also stained by the dye in a significant fraction of the population,

204 which suggested incorporation of the pilin subunit into the inner membrane. Another subfraction
205 appeared as fully unlabeled.

206 We considered two possible explanations for this unlabeled fraction. First, that production of
207 the pilus is a heterogeneous and potentially bistable phenotype in *A. baumannii* similar to
208 competence development in *B. subtilis* (53-55). Second, that the absence of cell body labelling
209 might be due to the production of pilus proteins that were not surface-exposed during the short
210 staining time window. While we previously demonstrated for *V. cholerae* that cysteine-containing
211 PilA subunits in the inner membrane were labeled even in the absence of the residual TFP
212 components (22), this was not the case for *C. crescentus* (49). In *C. crescentus*, only extended pili
213 and membrane-incorporated pilin subunits from pilus retraction events were labeled. It was argued
214 that this might be due to the size-based exclusion of the AF488-maleimide dye by the outer
215 membrane (49). While outer-membrane permeability and/or porins might differ between *V.*
216 *cholerae, C. crescentus,* and *A. baumannii*, we speculated that in the latter two organisms, cell-
217 surrounding capsular polysaccharides might also impede dye's access to the inner membrane-
218 incorporated pilin subunits. These capsular polysaccharides are considered a major virulence
219 determinant of *A. baumannii* (56) and could explain the lack of cell body staining in our images.
220 Upon further inspection of the A118 genome sequence, we identified a 22,663 bp genome stretch
221 between the genes *fkpA* and *lldP* that usually flank capsular biosynthesis clusters (56). BLAST
222 analysis of this cluster showed a 100% conservation of the gene order (18 genes in total) and a
223 99.2% pairwise sequence identity to the KL51 capsule biosynthesis gene cluster of *A. baumannii*
224 isolate WM98c (GenBank accession number MN148384; (57)), indicating that strain A118 is
225 indeed encapsulated.

To test our second hypothesis, we imaged a *pilT*-mutant derivative of strain A118-PilA[A61C]. Our underlying rationale was that pili that did extend would remain surface-exposed in this strain in the absence of the retraction ATPase PilT. Indeed, we observed many cells with multiple pili or bundles/clusters thereof (Fig. 2C). Interestingly, the cell bodies themselves were not labeled, which is consistent with the notion that pilus retraction was required to re-insert labeled pilin subunits into the inner membrane after they were pulled through the capsular material and the outer membrane secretin PilQ. However, this strain still showed labeling heterogeneity, which suggested that the pilus production was a phenotype in only a subfraction of the population. Interestingly, *A. baumannii* strains are known for a number of phase-variable controlled phenotypes including, for strain AB5075, cell morphology, biofilm formation, and surface motility (58), which is frequently linked to pili. Thus, we can speculate that the pilus-producing and non-producing bacteria within the population are phase variants that foster diverse phenotypes.

While *pilT* mutants are frequently hyperpiliated (24), the discovery of this in *A. baumannii* was somewhat surprising, as previous work noted the absence of pili in a *pilTU* mutant of strain ATCC 17978 (59). However, we must note that the absence of pili was scored by transmission electron microscopy in that study, which does not distinguish between diverse cell appendages, and that the fixation process might shear off pili. Interestingly, previous work had demonstrated that other *A. baumannii* strains produced both thin (~4 nm wide) and thick (~7 nm) pili (14). Notably, Wilharm *et al*. demonstrated that the thick pili were rarely observed on WT cells (only ~ 1 in 25–50 cells exposed such a pilus) though were frequently witnessed in a *pilT* deletion strain where each cell exposed one or several pili (14). These findings are consistent with the hyperpiliation phenotype described in this study. Indeed, our preliminary scanning electron micrographs of strain A118 supported the observation of multiple cell appendages of different

249 widths (some of those even in a *pilA*-minus strain), which motivated us to adapt the pilus-specific
250 thiol-labeling approach to unambiguously score only PilA-composed TFP.

251

252 **Competence and pili mutants are impaired in transformation**

253 To further investigate the link between pilus production and the strain's natural transformability,
254 we next generated a set of defined deletion strains. In this context, we also generated knock-out
255 strains of conserved competence genes that we considered to encode parts of the DNA-uptake
256 machinery based on common knowledge in other naturally competent bacteria (7, 60). Precisely,
257 we generated mutants where the gene products were required for the main steps of the DNA-uptake
258 and recombination process, namely the dynamic TFP (*pilA, pilQ, pilT, pilU*), DNA uptake and
259 translocation (*comEA, comF*), and ssDNA binding and recombination (*dprA, comM*) (Fig. 1A and
260 Table 3). We tested these mutants for natural transformation abilities and observed abrogation of
261 this process for all but two mutants, namely ΔpilU and ΔcomM (Fig. 3A). The lack of
262 transformation defects in the absence of *comM* was in line with the minor impact observed for
263 similar mutants in diverse *V. cholerae* strains (61, 62), given that the current transformation assay
264 was based on genomic DNA as transforming material that contained a resistance marker for
265 transformant scoring. In contrast, there was a significant decrease of the transformability in *comM*
266 mutants of *V. cholerae* and *A. baumannii* when PCR-amplified fragments served as transforming
267 material, which led to the exchange of single nucleotides or short stretches of DNA (27, 63). PilU,
268 on the other hand, is a secondary retraction ATPase (PilT is the primary enzyme) that is present in
269 many Gram-negative bacteria including *P. aeruginosa* in which it is essential for TFP-mediated
270 twitching motility (64). Related to natural competence, we previously showed that PilU of *V.*
271 *cholerae* was dispensable for DNA uptake and transformation (20), which is consistent with our

present findings (Fig. 3A). Interestingly, we and others recently demonstrated that *V. cholerae*'s PilU works solely in conjunction with PilT instead of compensating for the lack of PilT (51, 65), which suggests that it enhances the retraction force instead of behaving as an independent retraction enzyme, as was also suggested for *P. aeruginosa* (51, 65, 66).

We next established complementation assays to show causality between the lack of pilus or competence genes in this set of knock-out strains. Towards this goal, we cloned the genes downstream of the arabinose-inducible P_{BAD} promoter that was located on a miniTn7 transposon (22, 62). These genetically engineered constructs as well as the parental transposon without any gene inserted downstream of P_{BAD} (TnAraC) were then site-directly integrated into the respective strains (Table 1) and tested for their natural transformability. As shown in Figure 3B, complete or high levels of complementation were observed under arabinose-inducing conditions for strains lacking *pilT, comEA, comF*, or *dprA,* compared to the WT parental strain and its transposon-carrying derivative (grown in the absence or presence of arabinose). In contrast, complementation of the *pilA* and *pilQ* deletion strains was less efficient but could be boosted by an increase of the inducer arabinose (Fig. 3C). Collectively, these data confirmed that the transformation defects were caused by the gene-specific deletions and not secondary defects that might have occurred during strain engineering.

Pilus mutants are impaired in their surface motility

Recent studies are reporting considerable variations across *A. baumannii* strains that might also impact and explain their different surface mobilities. For example, considerable variations in amino acid sequences and glycosylation patterns of PilA proteins have been observed (strain A118 lacks the O-glycosylated C-terminal serine residue that is conserved in several other strains) (67-

69). Moreover, X-ray crystallography highlighted another key difference between *A. baumannii* PilA proteins, namely surface electrostatics, which could determine whether pili repulse or adhere to one another (69). Electrostatic adherence could trigger bundle formation, which would influence the strain's preference for biofilm formation over surface-dependent twitching motility. Given the correlation between TFP biosynthesis and natural transformation of strain A118 (Fig. 1), we queried whether deletion of the pilus and core competence genes would affect such surface-dependent movement. As shown in Figure 3D, we observed large variations in and between independent experiments, which could again be attributed to the species' phase variability that is known to impact surface motility (58). Nonetheless, motile versus non-motile strains were easily differentiable. We demonstrated that all *pil* mutants abrogated surface motility, while deletion of non-pilus competence genes did not impair surface movement. This finding contrasts previous reports by Wilharm *et al*., who showed that inactivation of both *pilT* and *comEC* abolished transformation and twitching-like motility in *A. baumannii* strains 07-095 and 07-102 (14). Interestingly, the *pilU* mutant had significantly impaired motility (Fig. 3D). This discrepancy between the *pilU* mutant's efficient transformability (Fig. 3A) and its inefficient surface motility (Fig. 3D) can be explained by the difference in requisite retraction force. While DNA uptake is unlikely to majorly constrain pilus retraction, the friction between the bacterial cell and the surface material likely requires enhanced force generation by the retraction motor PilT, which is accomplished through recruitment of and assistance by PilU. The absence of surface motility of the *pilU* mutant observed here for *A. baumannii* phenocopies that of *P. aeruginosa* (64). Despite this commonality between the two organisms, a recent study by Nolan *et al.* demonstrated that TFP were dispensable for low levels of natural transformation of *P. aeruginosa* (28), which

317 contrasted our findings. Here, we demonstrated that apart from PilU, the pilus components were
318 essential for *A. baumannii*'s natural transformability (Fig. 3A).

319

320 **TFP regulators impact transformation in *A. baumannii***

321 Given the parallels and discrepancies between *P. aeruginosa* and *A. baumannii,* we next
322 considered the impact of pilus-specific regulators on surface-dependent motility and
323 transformation of *A. baumannii*. We were especially interested in the PilSR TCS as well as the Pil-
324 Chp chemosensory systems (Fig. 4A), as homologs for these regulatory proteins exist in *A.*
325 *baumannii* (Table 3). Notably, Leong *et al*. recently showed that, while important for twitching
326 motility, these signal–transduction-related systems (e.g., PilS, PilR, and PilG) were fully
327 dispensable for natural transformation in *A. baylyi* (strains ADP1, BD413) (47), which was
328 recently confirmed for the Pil-Chp system (52). Given the differences we found in natural
329 transformability and TFP production between *A. baumannii* and *A. baylyi*, we were interested in
330 these systems in *A. baumannii*. In contrast to *A. baylyi*, deletion of *pilS* or *pilR* as well as *chpA* or
331 *pilG* in *A. baumannii* completely abolished transformation, while the absence of *pilH* did not
332 change the strain's transformation efficiency (Fig. 4B). Complementation restored natural
333 transformability in the mutants at regular (Fig. 4C) or elevated induction levels (Fig. 4D), except
334 for the *pilS* deletion strain, which could not be complemented under the tested conditions.
335 However, when we tested a *pilSR* double mutant, we restored its function through production of a
336 phosphomimetic PilR variant (D56E) while the native and unphosphorylated PilR was insufficient
337 for restoring transformation in the mutant (Fig. 4E). In contrast, both variants efficiently
338 complemented a *pilR* single knock-out in which the PilS protein was maintained to restore piliation
339 (Fig. 4F) and natural transformation (Fig. 4E). Therefore, these data confirm that PilS is required

for natural transformation in *A. baumannii* due to its phosphotransfer to PilR. Moreover, these data also suggest that the observed TFP production heterogeneity is not based on the level of phosphorylated PilR given that the phosphomimetic version should be expressed from the P_{BAD} promoter in the whole population.

Given the strong transformation phenotype of most of the regulatory mutants, we next tested their *pilA* transcript and PilA protein levels. For the *pilS* and *pilR* mutants, *pilA* expression levels were significantly reduced (Fig. 4G), and tagged PilA proteins were undetectable (Fig. 4H). On the contrary, the absence of *chpA, pilG,* or *pilH* significantly impacted neither the *pilA* transcript levels nor the PilA protein levels (Fig. 4G and H). We therefore speculated that the pilus assembly/disassembly might be impacted in the *chpA* and *pilG* mutants, which could explain their non-transformability (Fig. 4B). Hence, we combined the cysteine knock-in *pilA* allele with the various gene deletions and imaged potential pili in otherwise WT or *pilT*-minus background strains. Consistent with the absence of the major pilins in the Western blot analysis (Fig. 4H), neither pili nor the retracted inner–membrane-localized pilin subunit were detectable in the *pilS* and *pilR* mutants (Fig. 4I). Extended pili were also undetectable in the absence of ChpA and PilG. This is consistent with previous work in *P. aeruginosa* that showed production of the major pilin but no surface-exposed and therefore shearable pili when similar mutants were investigated. Nonetheless, in our experiments, fluorescent puncta were observed close to the cell surface, which suggests that these strains might initiate pilus elongation but are unable to assemble full length pili. This phenotype was partially reversed when the retraction enzyme PilT was absent, in which case extended pili/pilus bundles were visible (Fig. 4I). The labeling of the cell bodies of the *chpA* and *pilG* mutants by the thiol-reactive maleimide dye supports our idea that the initiation of pilus assembly takes place but that the very short pili seen as puncta in our images are quickly retracted

363 to transport the dye-labeled pilins back into the inner membrane. This phenotype might be caused
364 by an imbalanced PilH protein, which is known to enhance the function of PilT in *P. aeruginosa*
365 (36). This data is also in line with a previous observation that *chpA* and *pilG* mutants of *P.*
366 *aeruginosa* remained susceptible to pili-specific phage infections, which was not the case for an
367 extension-defective *pilB* mutant (36). The *pilH* mutant, on the other hand, had surface-exposed
368 long pili but contained fewer bacteria with labeled cell bodies compared to the WT conditions
369 (Fig. 4I). We therefore hypothesized that pilus elongation is favored over retraction through an
370 imbalanced PilG protein in this mutant.

371 Lastly, we tested the regulatory mutants for their ability to move on solid surfaces. As shown
372 in Figure 4J, all mutants of the two systems showed strong motility defects relative to the WT.
373 Interestingly, we observed that the *pilH* mutant exhibited strongly impaired surface motility
374 despite being piliated and fully transformable. This discrepancy between fully functional
375 transformation but a lack of proficient motility phenocopies the *pilU* mutant. These results suggest
376 that PilH might play a role in the recruitment or activation of PilU, potentially to enhance high-
377 force pilus retraction.

378

379 **CONCLUSION**

380 In this study, we sought to better understand how the poorly studied human pathogen *A. baumannii*
381 engages in horizontal gene transfer and, precisely, in natural competence for transformation. We
382 showed that *A. baumannii* has a tight time window of natural transformability under the tested
383 conditions, which correlated with the bacterium's TFP production. Consistent with this finding,
384 we demonstrated that this pilus is essential for the pathogen's natural transformation and that
385 regulatory circuits resembling those of *P. aeruginos*a play an important part in the production and

386 assembly of the TFP and therefore also natural transformation. Finally, we also supported previous
387 notions that retraction forces can be enhanced by the secondary retraction ATPase PilU, which is
388 dispensable for the DNA-uptake process.

389 Collectively, our data highlight that natural transformation dynamics and pilus regulation in *A.*
390 *baumannii* vastly differs from the model organism *A. baylyi*, which suggests that common
391 generalizations among these organisms should be taken with caution. Because *A. baumannii* is a
392 current and urgent threat to human health due to its frequent multi-drug resistance, it is important
393 to be able to predict how this pathogen is likely to mutate and the best ways of dealing with
394 infections when it does. Overall, this work sheds important light on mechanisms by which *A.*
395 *baumannii* can acquire foreign DNA, and therefore antimicrobial resistance genes, and will assist
396 both researchers and health care workers in better understanding the evolution of *A. baumannii*
397 as a public health threat.

398

399 **MATERIALS AND METHODS**

400 **Bacterial strains, plasmids, and culture conditions**

401 The bacterial strains and plasmids used in this study are listed in Table 1. Bacterial strains were
402 grown aerobically in Lysogeny broth medium (LB; 1% tryptone, 0.5% yeast extract, 1% sodium
403 chloride; Carl Roth, Germany) or on LB-agar plates at 37°C. For a selection of *Acinetobacter*
404 *baumannii* strains after bi- and tri-parental mating, CHROMagar™ Acinetobacter plates were
405 prepared following the manufacturer's instructions (CHROMagar, France).

406 For transformation assays, phosphate-buffered LB agar plates (pH 6.0) were used. For induction
407 of the P_{BAD} promoter, L-arabinose was added to the medium at a final concentration of 0.2% or
408 2%, as indicated.

409 The following antibiotics were used at these final concentrations whenever required: kanamycin
410 (50 μg/mL), gentamicin (15 μg/mL), and ampicillin (100 μg/mL).
411
412 **Long-read whole-genome sequencing (PacBio) and *de novo* assembly**
413 The isolation of genomic DNA (gDNA) and whole-genome sequencing was performed as
414 previously described (62) with minor modifications. Briefly, *A. baumannii* strain A118 (ATCC
415 BAA-2093) was back-diluted 1:100 from an overnight culture and grown aerobically in 25 mL LB
416 medium for 4h at 37°C (optical density at 600 nm [OD_{600}] 2.5–3.0). After 15 mL of this culture
417 was harvested by centrifugation, gDNA was isolated using Qiagen's Genomic DNA Buffer set
418 combined with a 500/G Genomic-tip. The alcohol-precipitated DNA was ultimately dissolved in
419 10 mM Tris/Cl buffer (pH 8.0). Further sample processing, sequencing, and *de novo* assembly
420 were performed by the Genomic Technology Facility of the University of Lausanne as described
421 (62). The assembled genome was annotated upon submission to the NCBI database using their
422 Prokaryotic Genome Annotation Pipeline (PGAP). The sequencing results are summarized in
423 Table 2.
424
425 **Genetic engineering of *Acinetobacter baumannii***
426 *A. baumannii* mutants or variants were constructed using a standard allelic exchange approach
427 with the counter-selectable suicide vectors pGP704-Sac28 or pGP704Sac-kan (70, 71).
428 Derivatives of these plasmids containing deletion constructs of the respective genes or site-directed
429 allele exchanges (of *pilA*) were transferred to *A. baumannii* through mating with *E. coli* S17-1λpir.
430 The deletion constructs were based on the PCR amplification of the flanking regions of the desired
431 genetic regions and, when needed, the *aph* cassette (Kan^R) as the selection marker using PWO

polymerase (Roche) or Q5 polymerase (BioLabs). Site-directed changes in the *pilA* allele were inserted using modified primers. The amplified fragments were joined by overlap extension PCR or Golden Gate assembly (72) and were cloned inside the suicide plasmids. The correct cloning products were screened for by colony PCR of the *E. coli* transformants (with GoTaq polymerase; Promega) and ultimately confirmed by Sanger sequencing (Microsynth, Switzerland).

Construction of inducible genes-of-interest was accomplished by placing the respective gene under control of the arabinose-inducible promoter P_{BAD} inside the miniTn7 transposon TnAraC (22, 62). The resulting transposons were transferred to the respective *A. baumannii* strains through a standard triparental mating approach (73).

Natural transformation assay

The transformation protocol used in this study was adapted from Harding *et al*. (15). Briefly, the bacteria were grown overnight in LB medium, back-diluted 1:100 into 2 mL of LB medium with or without 0.2% or 2% L-arabinose and were further cultured aerobically until they reached an OD_{600} of approximately 0.65. Next, 20 µL of the bacterial culture was mixed with 1 µg of isolated genomic DNA of strain A118Δ*hcp1::kan*, and 20 µL of this mixture was spotted onto pH-buffered LB agar plates (pH 6; without or with 0.2% or 2% arabinose). The plates were incubated for 2 h at 37°C. Following this incubation period, the cells were scraped off from the plate with a sterile loop and resuspended in 200 µL of LB medium. Serial dilutions were spotted in duplicate on kanamycin-containing LB agar plates to select the transformants and on plain LB agar plates to assess the total number of colony-forming units (CFUs). Transformation frequency was calculated as the CFU number of transformants divided by the total number of bacteria. Averages of at least two biologically independent experiments are provided. Transformation frequencies were log-

455 transformed (74) and statistically significant differences were determined as described in the figure
456 legends. When no transformants were recovered, the transformation frequencies were set to the
457 detection limit to allow the calculation of the average value of all biologically independent
458 replicates and for statistical analyses using the program Prism (GraphPad software; San Diego,
459 USA).
460
461 **TFP-dependent surface motility assay**
462 The bacterial strains were streaked on LB agar plates and incubated at 37°C overnight to obtain
463 single colonies. Bacterial material was retrieved from a single colony with a toothpick and gently
464 applied onto a freshly prepared 1% agar-only plate. The plates were sealed with parafilm and
465 incubated at 37°C for 4 days. Following the incubation, pictures of the plates were taken with a
466 M80 Stereo Zoom microscope equipped with a MC 170 HD camera (both from Leica). The
467 motility area was determined using the ImageJ software (imagej.nih.gov/ij/). Results of four
468 biological replicates consisting of three technical replicates for each strain are provided.
469 Significant differences were determined using Prism, as indicated in the figure legends.
470
471 **Gene expression determination using quantitative reverse transcription PCR (qRT-PCR)**
472 Back-diluted cultures were grown at 37°C in several parallel 2 mL LB medium-containing tubes
473 for the indicated amount of time (for the time course experiment) or up to an OD_{600} of 0.65. The
474 bacterial cells (1.5 mL to 8 mL; depending on the growth phase) were harvested by centrifugation
475 for 3 min at 4°C. The cell pellets were washed once with ice-cold PBS, resuspended in TRI reagent
476 (Sigma-Aldrich), vortexed for a few seconds, and then flash-frozen on dry ice before their storage
477 at -80°C. The RNA extraction, DNase treatment, reverse transcription, and quantitative PCR

(qPCR) were performed as previously described (76). Relative gene expression values were calculated based on normalization against the transcript levels of the housekeeping gene *gyrA*. Averages of at least three independent biological experiments are shown. Data were log-transformed (74) and statistical differences were assessed using the Prism software. Details on the statistical analyses are provided in the figure legends.

SDS-PAGE and Western blotting

To verify the production of PilA-FLAG proteins, cell lysates were prepared as described previously with minor modifications (75). Briefly, after overnight growth, the bacterial culture was back-diluted 1:100 in 2 mL of LB and grown at 37°C for the indicated amount of time (for time-course experiments) or up to an OD_{600} of ~0.65. At the time of harvesting, the bacteria were centrifuged for 3 min, and the pelleted cells were resuspended in 2x Laemmli buffer, whereby the volume was adjusted according to the total number of bacteria (100 µL buffer per OD_{600} unit). The resuspended samples were incubated at 95°C for 15 min. Proteins were separated by SDS-PAGE using 15% resolving gels and blotted onto PVDF membranes as previously described (76). Primary monoclonal antibodies against the FLAG-tag (ANTI-FLAG® M2; Sigma-Aldrich) were used at 1:2,000 dilution, and goat anti-mouse horseradish peroxidase (HRP) served as secondary antibody (diluted 1:5,000; Sigma-Aldrich). Sigma70 was detected as a loading control using Direct-Blot anti-*E. coli* Sigma70-HRP-conjugated antibodies at a dilution of 1:10,000 (BioLegend, USA distributed via Brunschwig, Switzerland). Lumi-Light^{PLUS} Western blotting substrate (Roche) served as the HRP substrate. Luminescent signals were detected using a ChemiDoc XRS+ station (BioRad).

501 **Microscopy**

502 Bacteria were grown until an OD_{600} of ~0.65 and then spotted onto thin agarose pads that were
503 mounted onto glass slides (1.2% agarose dissolved in 0.5x PBS). The cells were illuminated with
504 a HXP120 lamp and imaged through a Plan-Apochromat x100/NA 1.4 Ph3 oil objective by an
505 AxioCam MRm camera attached to an Axio Imager M2 epi-fluorescence microscope (Zeiss). The
506 Zeiss software ZEN 2.6 and ImageJ (imagej.nih.gov/ij/) were used for image acquisition and
507 analysis, respectively.

508

509 **Type IV pilus labeling**

510 Pilus labeling was performed as previously described with minor modifications (22, 49). Briefly,
511 genetically modified bacteria with modified *pilA* alleles (encoding for site-specific amino acid
512 changes to knock-in a new cysteine residue) were pre-grown overnight at 37°C, back-diluted 1:100
513 in 2 mL LB (supplemented without or with L-arabinose, as indicated), and grown at 37°C until an
514 OD_{600} of approximately 0.65. Alexa Fluor 488 C_5 maleimide (AF-488-Mal; Thermo Fisher
515 Scientific) was added to 100 µL of the bacterial culture at a final concentration of 25 µg/mL, gently
516 mixed, and incubated for 15 min at room temperature in the dark. Cells were subsequently
517 harvested by centrifugation (5,000 × g for 1 min.), washed once in 1x PBS, and resuspended in 30
518 µL of PBS before being imaged as described above.

519

520 **Data availability**

521 The assembled genome sequence as well as all raw data were deposited into NCBI under GenBank
522 accession number CP059039, BioSample number SAMN15507634, and the Sequence Read
523 Archive (SRA) accession number SUB7757186.

ACKNOWLEDGMENTS

We thank Sandrine Stutzmann for technical assistance, David W. Adams for advice on the cysteine knock-in strain engineering and pilus staining, members of the Blokesch group for fruitful discussions, and the staff of the Lausanne Genomic Technologies Facility at the University of Lausanne for sample processing, genome sequencing, and bioinformatic analysis.

This work was supported by the Swiss National Science Foundation in the context of the National Research Program 72 on Antimicrobial Resistance (grant 407240_167061). M.B. is a Howard Hughes Medical Institute (HHMI) International Research Scholar (grant 55008726).

REFERENCES

1. Rice LB. 2008. Federal funding for the study of antimicrobial resistance in nosocomial pathogens: no ESKAPE. J Infect Dis 197:1079-81.
2. Munoz-Price LS, Weinstein RA. 2008. *Acinetobacter* infection. N Engl J Med 358:1271-81.
3. Touchon M, Cury J, Yoon EJ, Krizova L, Cerqueira GC, Murphy C, Feldgarden M, Wortman J, Clermont D, Lambert T, Grillot-Courvalin C, Nemec A, Courvalin P, Rocha EP. 2014. The genomic diversification of the whole *Acinetobacter* genus: origins, mechanisms, and consequences. Genome Biol Evol 6:2866-82.
4. Lorenz MG, Wackernagel W. 1994. Bacterial gene transfer by natural genetic transformation in the environment. Microbiol Rev 58:563-602.
5. Johnston C, Martin B, Fichant G, Polard P, Claverys JP. 2014. Bacterial transformation: distribution, shared mechanisms and divergent control. Nat Rev Microbiol 12:181-96.
6. Seitz P, Blokesch M. 2013. Cues and regulatory pathways involved in natural competence and transformation in pathogenic and environmental Gram-negative bacteria. FEMS Microbiol Rev 37:336–363.
7. Dubnau D, Blokesch M. 2019. Mechanisms of DNA Uptake by Naturally Competent Bacteria. Annu Rev Genet 53:217-237.
8. Cooper RM, Tsimring L, Hasty J. 2017. Inter-species population dynamics enhance microbial horizontal gene transfer and spread of antibiotic resistance. Elife 6:pii: e25950.
9. Lin L, Ringel PD, Vettiger A, Durr L, Basler M. 2019. DNA Uptake upon T6SS-Dependent Prey Cell Lysis Induces SOS Response and Reduces Fitness of *Acinetobacter baylyi*. Cell Rep 29:1633-1644 e4.
10. Traglia GM, Quinn B, Schramm ST, Soler Bistue A, Ramirez MS. 2016. Serum albumin and Ca2+ are natural competence inducers in the human pathogen *Acinetobacter baumannii*. Antimicrob Agents Chemother doi:10.1128/AAC.00529-16.

11. Quinn B, Traglia GM, Nguyen M, Martinez J, Liu C, Fernandez JS, Ramirez MS. 2019. Effect of Host Human Products on Natural Transformation in *Acinetobacter baumannii*. Curr Microbiol 76:950-953.
12. Godeux AS, Lupo A, Haenni M, Guette-Marquet S, Wilharm G, Laaberki MH, Charpentier X. 2018. Fluorescence-Based Detection of Natural Transformation in Drug-Resistant *Acinetobacter baumannii*. J Bacteriol 200.
13. Ramirez MS, Don M, Merkier AK, Bistue AJ, Zorreguieta A, Centron D, Tolmasky ME. 2010. Naturally competent *Acinetobacter baumannii* clinical isolate as a convenient model for genetic studies. J Clin Microbiol 48:1488-90.
14. Wilharm G, Piesker J, Laue M, Skiebe E. 2013. DNA uptake by the nosocomial pathogen *Acinetobacter baumannii* occurs during movement along wet surfaces. J Bacteriol 195:4146-53.
15. Harding CM, Tracy EN, Carruthers MD, Rather PN, Actis LA, Munson RS, Jr. 2013. *Acinetobacter baumannii* strain M2 produces type IV pili which play a role in natural transformation and twitching motility but not surface-associated motility. mBio 4: e00360-13.
16. Wilharm G, Skiebe E. 2019. Methods for Natural Transformation in *Acinetobacter baumannii*. Methods Mol Biol 1946:75-85.
17. Carruthers MD, Harding CM, Baker BD, Bonomo RA, Hujer KM, Rather PN, Munson RS, Jr. 2013. Draft Genome Sequence of the Clinical Isolate *Acinetobacter nosocomialis* Strain M2. Genome Announc 1: e00906-13..
18. Wilharm G, Skiebe E, Higgins PG, Poppel MT, Blaschke U, Leser S, Heider C, Heindorf M, Brauner P, Jackel U, Bohland K, Cuny C, Lopinska A, Kaminski P, Kasprzak M, Bochenski M, Ciebiera O, Tobolka M, Zolnierowicz KM, Siekiera J, Seifert H, Gagne S, Salcedo SP, Kaatz M, Layer F, Bender JK, Fuchs S, Semmler T, Pfeifer Y, Jerzak L. 2017. Relatedness of wildlife and livestock avian isolates of the nosocomial pathogen *Acinetobacter baumannii* to lineages spread in hospitals worldwide. Environ Microbiol 19:4349-4364.
19. Meibom KL, Blokesch M, Dolganov NA, Wu C-Y, Schoolnik GK. 2005. Chitin induces natural competence in *Vibrio cholerae*. Science 310:1824-7.
20. Seitz P, Blokesch M. 2013. DNA-uptake machinery of naturally competent *Vibrio cholerae*. Proc Natl Acad Sci USA 110:17987-92.
21. Seitz P, Pezeshgi Modarres H, Borgeaud S, Bulushev RD, Steinbock LJ, Radenovic A, Dal Peraro M, Blokesch M. 2014. ComEA Is Essential for the Transfer of External DNA into the Periplasm in Naturally Transformable *Vibrio cholerae* Cells. PLoS Genet 10:e1004066.
22. Adams DW, Stutzmann S, Stoudmann C, Blokesch M. 2019. DNA-uptake pili of *Vibrio cholerae* are required for chitin colonization and capable of kin recognition via sequence-specific self-interaction. Nat Microbiol 4:1545-1557.
23. Ellison CK, Dalia TN, Vidal Ceballos A, Wang JC, Biais N, Brun YV, Dalia AB. 2018. Retraction of DNA-bound type IV competence pili initiates DNA uptake during natural transformation in Vibrio cholerae. Nat Microbiol 3:773-780.
24. Craig L, Forest KT, Maier B. 2019. Type IV pili: dynamics, biophysics and functional consequences. Nat Rev Microbiol 17:429-440.
25. Seitz P, Blokesch M. 2014. DNA transport across the outer and inner membranes of naturally transformable *Vibrio cholerae* is spatially but not temporally coupled. mBio 5: e01409-14.
26. Marie L, Rapisarda C, Morales V, Berge M, Perry T, Soulet AL, Gruget C, Remaut H, Fronzes R, Polard P. 2017. Bacterial RadA is a DnaB-type helicase interacting with RecA to promote bidirectional D-loop extension. Nat Commun 8:15638.

27. Nero TM, Dalia TN, Wang JC, Kysela DT, Bochman ML, Dalia AB. 2018. ComM is a hexameric helicase that promotes branch migration during natural transformation in diverse Gram-negative species. Nucleic Acids Res 46:6099-6111.
28. Nolan LM, Turnbull L, Katrib M, Osvath SR, Losa D, Lazenby JJ, Whitchurch CB. 2020. *Pseudomonas aeruginosa* is capable of natural transformation in biofilms. Microbiology 166:995-1003.
29. Ishimoto KS, Lory S. 1992. Identification of *pilR*, which encodes a transcriptional activator of the *Pseudomonas aeruginosa* pilin gene. J Bacteriol 174:3514-21.
30. Boyd JM, Koga T, Lory S. 1994. Identification and characterization of PilS, an essential regulator of pilin expression in *Pseudomonas aeruginosa*. Mol Gen Genet 243:565-74.
31. Hobbs M, Collie ES, Free PD, Livingston SP, Mattick JS. 1993. PilS and PilR, a two-component transcriptional regulatory system controlling expression of type 4 fimbriae in *Pseudomonas aeruginosa*. Mol Microbiol 7:669-82.
32. Kilmury SL, Burrows LL. 2016. Type IV pilins regulate their own expression via direct intramembrane interactions with the sensor kinase PilS. Proc Natl Acad Sci USA 113:6017-22.
33. Kilmury SLN, Burrows LL. 2018. The *Pseudomonas aeruginosa* PilSR Two-Component System Regulates Both Twitching and Swimming Motilities. mBio 9: e01310-18.
34. Whitchurch CB, Leech AJ, Young MD, Kennedy D, Sargent JL, Bertrand JJ, Semmler AB, Mellick AS, Martin PR, Alm RA, Hobbs M, Beatson SA, Huang B, Nguyen L, Commolli JC, Engel JN, Darzins A, Mattick JS. 2004. Characterization of a complex chemosensory signal transduction system which controls twitching motility in *Pseudomonas aeruginosa*. Mol Microbiol 52:873-93.
35. Graham KJ, Burrows LL. 2020. More than a feeling: microscopy approaches to understanding surface-sensing mechanisms. J Bacteriol doi:10.1128/JB.00492-20.
36. Bertrand JJ, West JT, Engel JN. 2010. Genetic analysis of the regulation of type IV pilus function by the Chp chemosensory system of *Pseudomonas aeruginosa*. J Bacteriol 192:994-1010.
37. Inclan YF, Persat A, Greninger A, Von Dollen J, Johnson J, Krogan N, Gitai Z, Engel JN. 2016. A scaffold protein connects type IV pili with the Chp chemosensory system to mediate activation of virulence signaling in *Pseudomonas aeruginosa*. Mol Microbiol 101:590-605.
38. Persat A, Inclan YF, Engel JN, Stone HA, Gitai Z. 2015. Type IV pili mechanochemically regulate virulence factors in *Pseudomonas aeruginosa*. Proc Natl Acad Sci U S A 112:7563-8.
39. Darzins A. 1994. Characterization of a *Pseudomonas aeruginosa* gene cluster involved in pilus biosynthesis and twitching motility: sequence similarity to the chemotaxis proteins of enterics and the gliding bacterium *Myxococcus xanthus*. Mol Microbiol 11:137-53.
40. Fulcher NB, Holliday PM, Klem E, Cann MJ, Wolfgang MC. 2010. The *Pseudomonas aeruginosa* Chp chemosensory system regulates intracellular cAMP levels by modulating adenylate cyclase activity. Mol Microbiol 76:889-904.
41. Silversmith RE, Wang B, Fulcher NB, Wolfgang MC, Bourret RB. 2016. Phosphoryl Group Flow within the Pseudomonas aeruginosa Pil-Chp Chemosensory System: DIFFERENTIAL FUNCTION OF THE EIGHT PHOSPHOTRANSFERASE AND THREE RECEIVER DOMAINS. J Biol Chem 291:17677-91.

42. Wolfgang MC, Lee VT, Gilmore ME, Lory S. 2003. Coordinate regulation of bacterial virulence genes by a novel adenylate cyclase-dependent signaling pathway. Dev Cell 4:253-63.
43. Juni E, Janik A. 1969. Transformation of *Acinetobacter calco-aceticus* (Bacterium anitratum). J Bacteriol 98:281-8.
44. Cruze JA, Singer JT, Finnerty WR. 1979. Conditions for Quantitative Transformation in *Acinetobacter calcoaceticus*. Curr Microbiol 3:129-132.
45. Porstendörfer, D., Gohl O, Mayer F, Averhoff B. 2000. ComP, a pilin-like protein essential for natural competence in *Acinetobacter* sp. Strain BD413: regulation, modification, and cellular localization. J Bacteriol 182:3673-80.
46. Ramirez MS, Adams MD, Bonomo RA, Centron D, Tolmasky ME. 2011. Genomic analysis of *Acinetobacter baumannii* A118 by comparison of optical maps: identification of structures related to its susceptibility phenotype. Antimicrob Agents Chemother 55:1520-6.
47. Leong CG, Bloomfield RA, Boyd CA, Dornbusch AJ, Lieber L, Liu F, Owen A, Slay E, Lang KM, Lostroh CP. 2017. The role of core and accessory type IV pilus genes in natural transformation and twitching motility in the bacterium *Acinetobacter baylyi*. PLoS One 12:e0182139.
48. Blair KM, Turner L, Winkelman JT, Berg HC, Kearns DB. 2008. A molecular clutch disables flagella in the *Bacillus subtilis* biofilm. Science 320:1636-8.
49. Ellison CK, Kan J, Dillard RS, Kysela DT, Ducret A, Berne C, Hampton CM, Ke Z, Wright ER, Biais N, Dalia AB, Brun YV. 2017. Obstruction of pilus retraction stimulates bacterial surface sensing. Science 358:535-538.
50. Kelley LA, Mezulis S, Yates CM, Wass MN, Sternberg MJ. 2015. The Phyre2 web portal for protein modeling, prediction and analysis. Nat Protoc 10:845-58.
51. Adams DW, Pereira JM, Stoudmann C, Stutzmann S, Blokesch M. 2019. The type IV pilus protein PilU functions as a PilT-dependent retraction ATPase. PLoS Genet 15:e1008393.
52. Ellison CK, Dalia TN, Shaevitz JW, Gitai Z, Dalia AB. 2020. Novel mechanisms of type IV pilus regulation in *Acinetobacter baylyi*. bioRxiv doi:10.1101/2020.09.28.317149:2020.09.28.317149.
53. Maamar H, Dubnau D. 2005. Bistability in the *Bacillus subtilis* K-state (competence) system requires a positive feedback loop. Mol Microbiol 56:615-24.
54. Smits WK, Eschevins CC, Susanna KA, Bron S, Kuipers OP, Hamoen LW. 2005. Stripping *Bacillus*: ComK auto-stimulation is responsible for the bistable response in competence development. Mol Microbiol 56:604-14.
55. Maamar H, Raj A, Dubnau D. 2007. Noise in gene expression determines cell fate in *Bacillus subtilis.* Science 317:526-9.
56. Singh JK, Adams FG, Brown MH. 2018. Diversity and Function of Capsular Polysaccharide in *Acinetobacter baumannii*. Front Microbiol 9:3301.
57. Wyres KL, Cahill SM, Holt KE, Hall RM, Kenyon JJ. 2020. Identification of *Acinetobacter baumannii* loci for capsular polysaccharide (KL) and lipooligosaccharide outer core (OCL) synthesis in genome assemblies using curated reference databases compatible with Kaptive. Microb Genom 6. doi: 10.1099/mgen.0.000339
58. Tipton KA, Dimitrova D, Rather PN. 2015. Phase-Variable Control of Multiple Phenotypes in *Acinetobacter baumannii* Strain AB5075. J Bacteriol 197:2593-9.

59. Tucker AT, Nowicki EM, Boll JM, Knauf GA, Burdis NC, Trent MS, Davies BW. 2014. Defining gene-phenotype relationships in *Acinetobacter baumannii* through one-step chromosomal gene inactivation. mBio 5:e01313-14.
60. Matthey N, Blokesch M. 2016. The DNA-Uptake Process of Naturally Competent *Vibrio cholerae*. Trends Microbiol 24:98-110.
61. Jaskólska M, Stutzmann S, Stoudmann C, Blokesch M. 2018. QstR-dependent regulation of natural competence and type VI secretion in *Vibrio cholerae*. Nucleic Acids Res 46:10619-10634.
62. Stutzmann S, Blokesch M. 2020. Comparison of chitin-induced natural transformation in pandemic *Vibrio cholerae* O1 El Tor strains. Environ Microbiol 22:4149-4166.
63. Godeux AS, Svedholm E, Lupo A, Haenni M, Venner S, Laaberki MH, Charpentier X. 2020. Scarless Removal of Large Resistance Island AbaR Results in Antibiotic Susceptibility and Increased Natural Transformability in *Acinetobacter baumannii*. Antimicrob Agents Chemother 64.
64. Chiang P, Sampaleanu LM, Ayers M, Pahuta M, Howell PL, Burrows LL. 2008. Functional role of conserved residues in the characteristic secretion NTPase motifs of the Pseudomonas aeruginosa type IV pilus motor proteins PilB, PilT and PilU. Microbiology 154:114-26.
65. Chlebek JL, Hughes HQ, Ratkiewicz AS, Rayyan R, Wang JC, Herrin BE, Dalia TN, Biais N, Dalia AB. 2019. PilT and PilU are homohexameric ATPases that coordinate to retract type IVa pili. PLoS Genet 15:e1008448.
66. Tala L, Fineberg A, Kukura P, Persat A. 2019. *Pseudomonas aeruginosa* orchestrates twitching motility by sequential control of type IV pili movements. Nat Microbiol 4:774-780.
67. Harding CM, Nasr MA, Kinsella RL, Scott NE, Foster LJ, Weber BS, Fiester SE, Actis LA, Tracy EN, Munson RS, Jr., Feldman MF. 2015. *Acinetobacter* strains carry two functional oligosaccharyltransferases, one devoted exclusively to type IV pilin, and the other one dedicated to O-glycosylation of multiple proteins. Mol Microbiol 96:1023-41.
68. Piepenbrink KH, Lillehoj E, Harding CM, Labonte JW, Zuo X, Rapp CA, Munson RS, Jr., Goldblum SE, Feldman MF, Gray JJ, Sundberg EJ. 2016. Structural Diversity in the Type IV Pili of Multidrug-resistant *Acinetobacter*. J Biol Chem 291:22924-22935.
69. Ronish LA, Lillehoj E, Fields JK, Sundberg EJ, Piepenbrink KH. 2019. The structure of PilA from *Acinetobacter baumannii* AB5075 suggests a mechanism for functional specialization in *Acinetobacter* type IV pili. J Biol Chem 294:218-230.
70. Meibom KL, Li XB, Nielsen AT, Wu CY, Roseman S, Schoolnik GK. 2004. The *Vibrio cholerae* chitin utilization program. Proc Natl Acad Sci USA 101:2524-9.
71. Metzger LC, Matthey N, Stoudmann C, Collas EJ, Blokesch M. 2019. Ecological implications of gene regulation by TfoX and TfoY among diverse *Vibrio* species. Environ Microbiol 21:2231-2247.
72. Engler C, Kandzia R, Marillonnet S. 2008. A one pot, one step, precision cloning method with high throughput capability. PLoS One 3:e3647.
73. Bao Y, Lies DP, Fu H, Roberts GP. 1991. An improved Tn7-based system for the single-copy insertion of cloned genes into chromosomes of Gram-negative bacteria. Gene 109:167-8.
74. Keene ON. 1995. The log transformation is special. Stat Med 14:811-9.
75. Metzger LC, Blokesch M. 2016. Regulation of competence-mediated horizontal gene transfer in the natural habitat of *Vibrio cholerae*. Curr Opin Microbiol 30:1-7.
76. Lo Scrudato M, Blokesch M. 2012. The regulatory network of natural competence and transformation of *Vibrio cholerae*. PLoS Genet 8:e1002778.

77. Craig L, Volkmann N, Arvai AS, Pique ME, Yeager M, Egelman EH, Tainer JA. 2006. Type IV pilus structure by cryo-electron microscopy and crystallography: implications for pilus assembly and functions. Mol Cell 23:651-62.
78. Matthey N, Drebes Dörr NC, Blokesch M. 2018. Long-Read-Based Genome Sequences of Pandemic and Environmental *Vibrio cholerae* Strains. Microbiol Resour Announc 7:e01574-18.
79. Traglia GM, Chua K, Centron D, Tolmasky ME, Ramirez MS. 2014. Whole-genome sequence analysis of the naturally competent *Acinetobacter baumannii* clinical isolate A118. Genome Biol Evol 6:2235-9.
80. Simon R, Priefer U, Pühler A. 1983. A broad host range mobilization system for *in vivo* genetic engineering: transposon mutagenesis in Gram negative bacteria. Nat Biotechnol 1:784-791.
81. Burrows LL. 2012. *Pseudomonas aeruginosa* twitching motility: type IV pili in action. Annu Rev Microbiol 66:493-520.
82. Heidelberg JF, Eisen JA, Nelson WC, Clayton RA, Gwinn ML, Dodson RJ, Haft DH, Hickey EK, Peterson JD, Umayam L, Gill SR, Nelson KE, Read TD, Tettelin H, Richardson D, Ermolaeva MD, Vamathevan J, Bass S, Qin H, Dragoi I, Sellers P, McDonald L, Utterback T, Fleishmann RD, Nierman WC, White O. 2000. DNA sequence of both chromosomes of the cholera pathogen *Vibrio cholerae*. Nature 406:477-83.
83. Barbe V, Vallenet D, Fonknechten N, Kreimeyer A, Oztas S, Labarre L, Cruveiller S, Robert C, Duprat S, Wincker P, Ornston LN, Weissenbach J, Marliere P, Cohen GN, Medigue C. 2004. Unique features revealed by the genome sequence of *Acinetobacter* sp. ADP1, a versatile and naturally transformation competent bacterium. Nucleic Acids Res 32:5766-79.
84. Winsor GL, Van Rossum T, Lo R, Khaira B, Whiteside MD, Hancock RE, Brinkman FS. 2009. *Pseudomonas* Genome Database: facilitating user-friendly, comprehensive comparisons of microbial genomes. Nucleic Acids Res 37:D483-8.

766 **FIGURE LEGENDS**

767 **Figure 1. Transformation is growth-phase dependent in *A. baumannii*. A)** Schematic
768 representation of DNA uptake machinery. Type IV pilus (TFP) components shown in blue, DNA
769 uptake and translocation proteins in orange, and proteins for binding and recombination of the
770 incoming ssDNA in green. **B)** Natural transformability of *A. baumannii* over time. The graph on
771 top shows the transformation frequencies, while the graph on the bottom depicts the growth of the
772 bacteria given as in optical density at 600 nm (OD_{600}) units. **C)** Relative expression values over
773 time for a subset of competence genes (*pilA*, *pilQ*, *pilT*, *comEA*, *comEC,* and *dprA*). **D)**
774 Transformation frequencies of the wild-type (WT) and the strain encoding the PilA-FLAG
775 translational fusion. **E-F)** Immunoblotting of FLAG-tagged PilA at different time points through
776 the bacterial growth phases (as indicated in minutes) in the *pilA*-FLAG strain (D) or its *pilQ*-
777 negative derivative (*pilA*-FLAGΔ*pilQ*) (E). Detection of Sigma70 served as loading control. Two
778 and three biologically independent experiments were performed for panels (B) and (C-F),
779 respectively, and the mean values (±SD) are shown for all graphs. <, below detection limit.
780 Statistical analyses were performed on log-transformed data. Statistics was based on (C) a two-
781 way ANOVA test with Tukey's multiple comparisons (time points compared to 90 min, as
782 indicated by the box in the legend) or (D) an unpaired *t* test with Welch's correction. **P*<0.05,
783 ***P*<0.01, ****P*<0.001.

784

785 **Figure 2. Design and functionality of PilA cysteine knock-in variants. A**) 3D structural model
786 of the *Neisseria gonorrhoeae* major type IV pilin PilE (PDB, 2HI2; (77)), which is shown
787 alongside Phyre2 (50) structural predictions of the major pilin PilA of pandemic *V. cholerae* and
788 of PilA of *A. baumannii* strain A118 (this study). The conserved αβ–loops are shown in greenish-

789 yellow and the residue chosen for the cysteine exchange (A61) is shown in red. Bottom panel:
790 Sequence alignments of *N. gonorrhoeae* PilE (Ng, Uniprot; P02974), *V. cholerae* PilA (Vc; protein
791 ID AWB74893.1 (78)) and *A. baumannii* PilA (Ab; strain A118 & protein ID H0N27_01510)
792 using Clustal Omega. The αβ–loop is coloured in yellow. The functional cysteine substitution in
793 *V. cholerae'*s PilA is highlighted (S67; (22)). Residues tested in *A. baumannii* in this study are
794 shown in bold and underlined. **B)** Natural transformability of PilA cysteine knock-in variants. Bars
795 show the average transformation frequency of three independent experiments (±SD). Statistical
796 analyses were performed on log-transformed data using a one-way ANOVA followed by Sidak's
797 multiple comparisons test. Each mutant strain is compared to the WT strain. #, under detection
798 limit in at least one experiment, in which case the detection limit was used for the calculation of
799 the average value and statistical analyses. $^{**}P<0.01$, $^{***}P<0.001$, $^{****}P<0.0001$. **C)** Pilus
800 imaging using a thiol-reactive maleimide dye. Snapshot images of A118-*pilA*[A61C] and A118-
801 *pilA*[A61C]Δ*pilT* and the parental WT strain. The ΔpilA strain served as an additional negative
802 control. The bacteria were stained with AF-488-Mal and imaged in the phase contrast (PC) or
803 green fluorescence (Dye) channels. A merged image of both channels is shown in the bottom row
804 (Merge). The contrast of the merged images was adjusted for best pilus visualization. An
805 enlargement of the marked region (dotted boxes) is shown as an inset. Bar = 5 µm.
806
807 **Figure 3. Type IV pilus genes are essential for transformation and surface motility. A-C)**
808 Transformation frequencies of defined mutants (details as in Fig. 1). For complementation, the
809 strains carried a transposon without (control, TnAraC; no gene downstream of P_{BAD} promoter) or
810 with (TnXXXX) the complementing gene on their chromosome and were grown in the absence or
811 presence of 0.2% (B) or 2% (C) arabinose. For all bar plots, transformation frequencies of three

812 independent experiments are plotted as mean values (±SD). <, below detection limit. #, under d.l.
813 in at least one replicate (d.l. used for calculation of mean value). Log-transformed data was used
814 for statistical analysis. When no transformants were obtained, the mean of the detection limit (d.l.)
815 was used for statistical analyses. **D)** TFP mutants are non-motile on solid surfaces. Surface motility
816 of the mutants described in panel A is depicted on the *Y*-axis based on the occupied area on the
817 motility plates. Four biological experiments with three technical replicates are shown for each
818 strain (n=12). Images from one experimental set are shown below the graph. Statistical analyses:
819 (A-C) One-way ANOVA, using Sidak's multiple comparisons test; (D) Brown-Forsythe and
820 Welch ANOVA tests with unpaired t with Welch's correction. *P<0.05, ****P<0.0001, n.s., not
821 significant. The strains were compared to the WT (A, D) or the most appropriate control strain
822 (boxed strain name in B and C).
823
824 **Figure 4.** The *A. baumannii* PilSR and Pil-Chp systems are required for natural transformation
825 and surface motility. **A)** Schematic representation of the PilSR and Pil-Chp systems. Left (gray):
826 Upon activation, PilS phosphorylates PilR, which promotes expression of *pilA*. Right (purple): PilJ
827 promotes auto-phosphorylation of ChpA, which subsequently phosphorylates PilG and/or PilH,
828 resulting in increased or decreased cAMP levels, respectively. PilG and PilH were also proposed
829 to foster T4P extension or retraction. **B-E)** Transformability of TFP regulation mutants without or
830 with complementing constructs ± inducer, as indicated. Details as in Fig. 3. The WT and WT-
831 TnAraC served as controls. Transformation frequencies are shown as mean value (±SD) of three
832 independent experiments. <, below detection limit (d.l.). For statistical analyses, a one-way
833 ANOVA with Sidak's multiple comparisons test was performed on log-transformed data and the
834 different strains' values were compared to the WT (B) or to the most appropriate control strain

(boxed name in C-E). #, under detection limit in at least one replicate. *P<0.05, ****P<0.0001, n.s. = not significant. **F + H)** Imaging of TFP in the regulatory mutants. PilA[A61C] pilus imaging of *pilT*-positive or *pilT*-negative strains (as indicated). For F) The strains were *pilR*-positive or *pilR*-negative and carried complementing *pilR* or its phosphomimetic *pilR*[D56E] variant on a transposon, as indicated. For H) The strains were deleted for the regulatory gene that is indicated above each column. Details as in Fig. 2, with the exception that only the merged images are shown. Bar = 5 µm (enlarged images are 2x magnified). **G)** Relative expression of *pilA* in the regulatory mutants. Average values (±SD) of two independent experiments are shown and statistics reflect a two-way ANOVA with Tukey's multiple comparisons test in which each strain was compared to the WT. **P<0.01, n.s. = not significant. **H)** Detection of PilA-FLAG in the different regulatory mutants. Representative images of two independent replicates. Details as in Fig. 1. **J)** TFP regulatory mutants are non-motile. The surface motility of the PilSR/ChpA system mutants is shown. Details as in Fig. 3D. The motility values of each strain were compared to the WT using Brown-Forsythe and Welch ANOVA tests with unpaired t with Welch's correction. **P<0.01.

TABLES

Table 1: Bacterial strains and plasmids used in this study

Strains or plasmids	Genotype/description	Internal strain number	Reference (original strain and genome sequence)
A. baumannii			
A118	Wild type; Amp^R, Cm^R	MB#5144	(13, 79); this study
A118Δhcp1::kan	A118 with *hcp1* replaced by *aph* cassette, using pGP704-Sac28-Δhcp1::kan (A118Δ*hcp1*::*aph*); Amp^R, Cm^R	MB#6403	This study
A118-pilA-FLAG	A118 carrying translational fusion encoding *pilA*-FLAG allele at native pilA locus; Amp^R, Cm^R	MB#8859	This study
A118-pilA-FLAGΔpilQ	A118-pilA-FLAG with *pilQ* deleted, using suicide plasmid pGP704-Sac-Kan-ΔpilQ; Amp^R, Cm^R	MB#8860	This study
A118ΔpilA	A118 with *pilA* deleted, using suicide plasmid pGP704-Sac-Kan-ΔpilA; Amp^R, Cm^R	MB#8585	This study
A118ΔpilQ	A118 with *pilQ* deleted, using suicide plasmid pGP704-Sac-Kan-ΔpilQ; Amp^R, Cm^R	MB#8584	This study
A118ΔpilT	A118 with *pilT* deleted, using suicide plasmid pGP704-Sac-Kan-ΔpilT; Amp^R, Cm^R	MB#8586	This study
A118ΔpilU	A118 with *pilU* deleted, using suicide plasmid pGP704-Sac-Kan-ΔpilU; Amp^R, Cm^R	MB#8861	This study
A118ΔcomEA	A118 with *comEA* deleted, using suicide plasmid pGP704-Sac-Kan-ΔcomEA; Amp^R, Cm^R	MB#8862	This study
A118ΔcomF	A118 with *comF* deleted, using suicide plasmid pGP704-Sac-Kan-ΔcomF; Amp^R, Cm^R	MB#8863	This study
A118ΔdprA	A118 with *dprA* deleted, using suicide plasmid pGP704-Sac-Kan-ΔdprA; Amp^R, Cm^R	MB#8864	This study
A118ΔcomM	A118 with *comM* deleted, using suicide plasmid pGP704-Sac-Kan-ΔcomM; Amp^R, Cm^R	MB#8865	This study
A118-TnAraC	A118 containing mini-Tn7-*araC* (TnAraC); Amp^R, Cm^R, $Gent^R$	MB#8874	This study
A118ΔpilA-TnAraC	A118ΔpilA containing mini-Tn7-*araC* (TnAraC); Amp^R, Cm^R, $Gent^R$	MB#8875	This study
A118ΔpilA-TnPilA	A118ΔpilA containing mini-Tn7-*araC-pilA* (TnPilA); Amp^R, Cm^R, $Gent^R$	MB#8866	This study
A118ΔpilQ-TnAraC	A118ΔpilQ containing mini-Tn7-*araC* (TnAraC); Amp^R, Cm^R, $Gent^R$	MB#8876	This study
A118ΔpilQ-TnPilQ	A118ΔpilQ containing mini-Tn7-*araC-pilQ* (TnPilQ); Amp^R, Cm^R, $Gent^R$	MB#8867	This study
A118ΔpilT-TnAraC	A118ΔpilT containing mini-Tn7-*araC* (TnAraC); Amp^R, Cm^R, $Gent^R$	MB#8877	This study
A118ΔpilT-TnPilT	A118ΔpilT containing mini-Tn7-*araC-pilT* (TnPilT); Amp^R, Cm^R, $Gent^R$	MB#8868	This study
A118ΔpilU-TnAraC	A118ΔpilU containing mini-Tn7-*araC* (TnAraC); Amp^R, Cm^R, $Gent^R$	MB#8878	This study
A118ΔpilU-TnPilU	A118ΔpilU containing mini-Tn7-*araC-pilU* (TnPilU); Amp^R, Cm^R, $Gent^R$	MB#8869	This study

A118ΔcomEA-TnAraC	A118ΔcomEA containing mini-Tn7-*araC* (TnAraC); Amp^R, Cm^R, $Gent^R$	MB#8879	This study
A118ΔcomEA-TnComEA	A118ΔcomEA containing mini-Tn7-*araC-comEA* (TnComEA); Amp^R, Cm^R, $Gent^R$	MB#8870	This study
A118ΔcomF-TnAraC	A118ΔcomF containing mini-Tn7-*araC* (TnAraC); Amp^R, Cm^R, $Gent^R$	MB#8880	This study
A118ΔcomF-TnComF	A118ΔcomF containing mini-Tn7-*araC-comF* (TnComF); Amp^R, Cm^R, $Gent^R$	MB#8871	This study
A118ΔdprA-TnAraC	A118ΔdprA containing mini-Tn7-*araC* (TnAraC); Amp^R, Cm^R, $Gent^R$	MB#8881	This study
A118ΔdprA-TnDprA	A118ΔdprA containing mini-Tn7-*araC-dprA* (TnDprA); Amp^R, Cm^R, $Gent^R$	MB#8872	This study
A118ΔcomM-TnAraC	A118ΔcomM containing mini-Tn7-*araC* (TnAraC); Amp^R, Cm^R, $Gent^R$	MB#8882	This study
A118ΔcomM-TnComM	A118ΔcomM containing mini-Tn7-*araC-comM* (TnComM); Amp^R, Cm^R, $Gent^R$	MB#8873	This study
A118ΔpilS	A118 with *pilS* deleted, using suicide plasmid pGP704-Sac-Kan-ΔpilS; Amp^R, Cm^R	MB#8590	This study
A118ΔpilR	A118 with *pilR* deleted, using suicide plasmid pGP704-Sac-Kan-ΔpilR; Amp^R, Cm^R	MB#8591	This study
A118ΔchpA	A118 with *chpA* deleted, using suicide plasmid pGP704-Sac-Kan-ΔchpA; Amp^R, Cm^R	MB#8588	This study
A118ΔpilG	A118 with *pilG* deleted, using suicide plasmid pGP704-Sac-Kan-ΔpilG; Amp^R, Cm^R	MB#8587	This study
A118ΔpilH	A118 with *pilH* deleted, using suicide plasmid pGP704-Sac-Kan-ΔpilH; Amp^R, Cm^R	MB#8589	This study
A118ΔpilS-TnAraC	A118ΔpilS containing mini-Tn7-*araC* (TnAraC); Amp^R, Cm^R, $Gent^R$	MB#8888	This study
A118ΔpilS-TnPilS	A118ΔpilS containing mini-Tn7-*araC-pilS* (TnPilS); Amp^R, Cm^R, $Gent^R$	MB#8883	This study
A118ΔpilR-TnAraC	A118ΔpilR containing mini-Tn7-*araC* (TnAraC); Amp^R, Cm^R, $Gent^R$	MB#8889	This study
A118ΔpilR-TnPilR	A118ΔpilR containing mini-Tn7-*araC-pilR* (TnPilR); Amp^R, Cm^R, $Gent^R$	MB#8884	This study
A118ΔchpA-TnAraC	A118ΔchpA containing mini-Tn7-*araC* (TnAraC); Amp^R, Cm^R, $Gent^R$	MB#8890	This study
A118ΔchpA-TnChpA	A118ΔchpA containing mini-Tn7-*araC-chpA* (TnChpA); Amp^R, Cm^R, $Gent^R$	MB#8885	This study
A118ΔpilG-TnAraC	A118ΔpilG containing mini-Tn7-*araC* (TnAraC); Amp^R, Cm^R, $Gent^R$	MB#8891	This study
A118ΔpilG-TnPilG	A118ΔpilG containing mini-Tn7-*araC-pilG* (TnPilG); Amp^R, Cm^R, $Gent^R$	MB#8886	This study
A118ΔpilH-TnAraC	A118ΔpilH containing mini-Tn7-*araC* (TnAraC); Amp^R, Cm^R, $Gent^R$	MB#8892	This study
A118ΔpilH-TnPilH	A118ΔpilH containing mini-Tn7-*araC-pilH* (TnPilH); Amp^R, Cm^R, $Gent^R$	MB#8887	This study
A118-pilA-FLAGΔpilS	A118-pilA-FLAG with *pilS* deleted, using suicide plasmid pGP704-Sac-Kan-ΔpilS; Amp^R, Cm^R	MB#8893	This study
A118-pilA-FLAGΔpilR	A118-pilA-FLAG with *pilR* deleted, using suicide plasmid pGP704-Sac-Kan-ΔpilR; Amp^R, Cm^R	MB#8894	This study
A118-pilA-FLAGΔchpA	A118-pilA-FLAG with *chpA* deleted, using suicide plasmid pGP704-Sac-Kan-ΔchpA; Amp^R, Cm^R	MB#8895	This study
A118-pilA-FLAGΔpilG	A118-pilA-FLAG with *pilG* deleted, using suicide plasmid pGP704-Sac-Kan-ΔpilG; Amp^R, Cm^R	MB#8896	This study

A118-pilA-FLAGΔpilH	A118-pilA-FLAG with *pilH* deleted, using suicide plasmid pGP704-Sac-Kan-ΔpilH; Amp^R, Cm^R	MB#8897	This study
A118-pilA[A61C]	A118 with site-directed point mutation in *pilA* (resulting in PilA[A61C]); Amp^R, Cm^R	MB#8898	This study
A118-pilA[G60C]	A118 with site-directed point mutation in *pilA* (resulting in PilA[G60C]); Amp^R, Cm^R	MB#8918	This study
A118-pilA[V62C]	A118 with site-directed point mutation in *pilA* (resulting in PilA[V62C]); Amp^R, Cm^R	MB#8919	This study
A118-pilA[T64C]	A118 with site-directed point mutation in *pilA* (resulting in PilA[T64C]); Amp^R, Cm^R	MB#8920	This study
A118-pilA[S67C]	A118 with site-directed point mutation in *pilA* (resulting in PilA[S67C]); Amp^R, Cm^R	MB#8921	This study
A118-pilA[T72C]	A118 with site-directed point mutation in *pilA* (resulting in PilA[T72C]); Amp^R, Cm^R	MB#8922	This study
A118-pilA[T75C]	A118 with site-directed point mutation in *pilA* (resulting in PilA[T75C]); Amp^R, Cm^R	MB#8923	This study
A118-pilA[A61C]ΔpilS	A118-pilA[A61C] with *pilS* deleted, using suicide plasmid pGP704-Sac-Kan-ΔpilS; Amp^R, Cm^R	MB#8899	This study
A118-pilA[A61C]ΔpilR	A118-pilA[A61C] with *pilR* deleted, using suicide plasmid pGP704-Sac-Kan-ΔpilR; Amp^R, Cm^R	MB#8900	This study
A118-pilA[A61C]ΔchpA	A118-pilA[A61C] with *chpA* deleted, using suicide plasmid pGP704-Sac-Kan-ΔchpA; Amp^R, Cm^R	MB#8901	This study
A118-pilA[A61C]ΔpilG	A118-pilA[A61C] with *pilG* deleted, using suicide plasmid pGP704-Sac-Kan-ΔpilG; Amp^R, Cm^R	MB#8902	This study
A118-pilA[A61C]ΔpilH	A118-pilA[A61C] with *pilH* deleted, using suicide plasmid pGP704-Sac-Kan-ΔpilH; Amp^R, Cm^R	MB#8903	This study
A118-pilA[A61C]ΔpilT	A118-pilA[A61C] with *pilT* deleted, using suicide plasmid pGP704-Sac-Kan-ΔpilT; Amp^R, Cm^R	MB#8904	This study
A118-pilA[A61C] ΔpilTΔpilS	A118-pilA[A61C]ΔpilT with *pilS* deleted, using suicide plasmid pGP704-Sac-Kan-ΔpilS; Amp^R, Cm^R	MB#8905	This study
A118-pilA[A61C] ΔpilTΔpilR	A118-pilA[A61C]ΔpilT with *pilR* deleted, using suicide plasmid pGP704-Sac-Kan-ΔpilR; Amp^R, Cm^R	MB#8906	This study
A118-pilA[A61C] ΔpilTΔchpA	A118-pilA[A61C]ΔpilT with *chpA* deleted, using suicide plasmid pGP704-Sac-Kan-ΔchpA; Amp^R, Cm^R	MB#8907	This study
A118-pilA[A61C] ΔpilTΔpilG	A118-pilA[A61C]ΔpilT with *pilG* deleted, using suicide plasmid pGP704-Sac-Kan-ΔpilG; Amp^R, Cm^R	MB#8908	This study
A118-pilA[A61C] ΔpilTΔpilH	A118-pilA[A61C]ΔpilT with *pilH* deleted, using suicide plasmid pGP704-Sac-Kan-ΔpilH; Amp^R, Cm^R	MB#8909	This study
A118ΔpilR-TnPilR-D56E	A118ΔpilR containing mini-Tn7-*araC-pilR*[D56E] (TnPilR[D56E]); Amp^R, Cm^R, $Gent^R$	MB#8910	This study
A118ΔpilSR	A118 with *pilSR* deleted, using suicide plasmid pGP704-Sac-Kan-ΔpilSR; Amp^R, Cm^R	MB#8911	This study
A118ΔpilSR-TnAraC	A118 ΔpilSR containing mini-Tn7-*araC* (TnAraC); Amp^R, Cm^R, $Gent^R$	MB#8912	This study
A118ΔpilSR-TnPilR	A118ΔpilSR containing mini-Tn7-*araC-pilR* (TnPilR); Amp^R, Cm^R, $Gent^R$	MB#8913	This study
A118ΔpilSR-TnPilR[D56E]	A118ΔpilSR containing mini-Tn7-*araC-pilR*[D56E] (TnPilR[D56E]); Amp^R, Cm^R, $Gent^R$	MB#8914	This study

A118-pilA[A61C]ΔpilTΔpilR-TnAraC	A118-pilA[A61C]ΔpilTΔpilR containing mini-Tn7-*araC* (TnAraC); Amp^R, Cm^R, $Gent^R$	MB#8915	This study
A118-pilA[A61C]ΔpilTΔpilR-TnPilR	A118-pilA[A61C]ΔpilTΔpilR containing mini-Tn7-*araC-pilR* (TnPilR); Amp^R, Cm^R, $Gent^R$	MB#8916	This study
A118-pilA[A61C]ΔpilTΔpilR-TnPilR[D56E]	A118-pilA[A61C]ΔpilTΔpilR containing mini-Tn7-*araC-pilR*[D56E] (TnPilR[D56E]); Amp^R, Cm^R, $Gent^R$	MB#8917	This study
E. coli			
S17-1λpir	Tp^R Sm^R *recA, thi, pro, hsdR2M1*, RP4:2-Tc:Mu:Km^R, Tn7 (λpir)	MB#648	(80)
Plasmids			
pGP704-Sac28	Suicide plasmid, ori R6K *sacB*; Amp^R	MB#649	(70)
pGP704-Sac-Kan	Suicide plasmid, ori R6K *sacB*; Kan^R	MB#6038	(71)
pGP704-TnAraC	pGP704 with mini-Tn7 carrying *araC* and P_{BAD}; Amp^R, $Gent^R$	MB#5513	(22, 62)
pUX-BF-13	*ori*R6K, helper plasmid with Tn7 transposition function; Amp^R	MB#457	(73)
pGP704-Sac28-Δhcp::kan	pGP704-Sac28 carrying *hcp* with an insertion of *aph;* Amp^R, Kan^R	MB#8924	This study
pGP704-Sac-Kan-pilA-FLAG	pGP704-Sac-Kan carrying the *pilA*-FLAG allele with flanking regions; Kan^R	MB#8925	This study
pGP704-Sac-Kan-ΔpilQ	pGP704-Sac-Kan carrying a deletion within *pilQ;* Kan^R	MB#8926	This study
pGP704-Sac-Kan-ΔpilA	pGP704-Sac-Kan carrying a deletion within *pilA*; Kan^R	MB#8927	This study
pGP704-Sac-Kan-ΔpilT	pGP704-Sac-Kan carrying a deletion within *pilT*; Kan^R	MB#8928	This study
pGP704-Sac-Kan-ΔpilU	pGP704-Sac-Kan carrying a deletion within *pilU;* Kan^R	MB#8929	This study
pGP704-Sac-Kan-ΔcomEA	pGP704-Sac-Kan carrying a deletion within *comEA*; Kan^R	MB#8930	This study
pGP704-Sac-Kan-ΔcomF	pGP704-Sac-Kan carrying a deletion within *comF*; Kan^R	MB#8931	This study
pGP704-Sac-Kan-ΔdprA	pGP704-Sac-Kan carrying a deletion within *dprA*; Kan^R	MB#8932	This study
pGP704-Sac-Kan-ΔcomM	pGP704-Sac-Kan carrying a deletion within *comM*; Kan^R	MB#8933	This study
pGP704-TnPilA	pGP704 with mini-Tn7 carrying *araC* and P_{BAD}-driven *pilA*; Amp^R, $Gent^R$	MB#8934	This study
pGP704-TnPilQ	pGP704 with mini-Tn7 carrying *araC* and P_{BAD}-driven *pilQ*; Amp^R, $Gent^R$	MB#8935	This study
pGP704-TnPilT	pGP704 with mini-Tn7 carrying *araC* and P_{BAD}-driven *pilT*; Amp^R, $Gent^R$	MB#8936	This study
pGP704-TnPilU	pGP704 with mini-Tn7 carrying *araC* and P_{BAD}-driven *pilU*; Amp^R, $Gent^R$	MB#8937	This study
pGP704-TnComEA	pGP704 with mini-Tn7 carrying *araC* and P_{BAD}-driven *comEA*; Amp^R, $Gent^R$	MB#8938	This study
pGP704-TnComF	pGP704 with mini-Tn7 carrying *araC* and P_{BAD}-driven *comF*; Amp^R, $Gent^R$	MB#8939	This study
pGP704-TnDprA	pGP704 with mini-Tn7 carrying *araC* and P_{BAD}-driven *dprA*; Amp^R, $Gent^R$	MB#8940	This study
pGP704-TnComM	pGP704 with mini-Tn7 carrying *araC* and P_{BAD}-driven *comM*; Amp^R, $Gent^R$	MB#8941	This study

pGP704-Sac-Kan-ΔpilS	pGP704-Sac-Kan carrying a deletion within *pilS*; Kan^R	MB#8942	This study
pGP704-Sac-Kan-ΔpilR	pGP704-Sac-Kan carrying a deletion within *pilR*; Kan^R	MB#8943	This study
pGP704-Sac-Kan-ΔchpA	pGP704-Sac-Kan carrying a deletion within *chpA*; Kan^R	MB#8944	This study
pGP704-Sac-Kan-ΔpilG	pGP704-Sac-Kan carrying a deletion within *pilG*; Kan^R	MB#8945	This study
pGP704-Sac-Kan-ΔpilH	pGP704-Sac-Kan carrying a deletion within *pilH*; Kan^R	MB#8946	This study
pGP704-TnPilS	pGP704 with mini-Tn7 carrying *araC* and P_{BAD}-driven *pilS*; Amp^R, $Gent^R$	MB#8947	This study
pGP704-TnPilR	pGP704 with mini-Tn7 carrying *araC* and P_{BAD}-driven *pilR*; Amp^R, $Gent^R$	MB#8948	This study
pGP704-TnChpA	pGP704 with mini-Tn7 carrying *araC* and P_{BAD}-driven *chpA*; Amp^R, $Gent^R$	MB#8949	This study
pGP704-TnPilG	pGP704 with mini-Tn7 carrying *araC* and P_{BAD}-driven *pilG*; Amp^R, $Gent^R$	MB#8950	This study
pGP704-TnPilH	pGP704 with mini-Tn7 carrying *araC* and P_{BAD}-driven *pilH*; Amp^R, $Gent^R$	MB#8951	This study
pGP704-Sac-Kan-pilA[A61C]	pGP704-Sac-Kan carrying a genome fragment resulting in a site-directed point mutation in *pilA* (resulting in PilA[A61C]); Kan^R	MB#8952	This study
pGP704-TnPilR[D56E]	pGP704 with mini-Tn7 carrying *araC* and P_{BAD}-driven *pilR*[D56E]; Amp^R, $Gent^R$	MB#8953	This study
pGP704-Sac-Kan-delta-pilSR	pGP704-Sac-Kan carrying a deletion within *pilSR;* Kan^R	MB#8954	This study
pGP704-Sac-Kan-pilA[G60C]	pGP704-Sac-Kan carrying a genome fragment resulting in a site-directed point mutation in *pilA* (resulting in PilA[G60C]); Kan^R	MB#8955	This study
pGP704-Sac-Kan-pilA[V62C]	pGP704-Sac-Kan carrying a genome fragment resulting in a site-directed point mutation in *pilA* (resulting in PilA[V62C]); Kan^R	MB#8956	This study
pGP704-Sac-Kan-pilA[T64C]	pGP704-Sac-Kan carrying a genome fragment resulting in a site-directed point mutation in *pilA* (resulting in PilA[T64C]); Kan^R	MB#8957	This study
pGP704-Sac-Kan-pilA[S67C]	pGP704-Sac-Kan carrying a genome fragment resulting in a site-directed point mutation in *pilA* (resulting in PilA[S67C]); Kan^R	MB#8958	This study
pGP704-Sac-Kan-pilA[T72C]	pGP704-Sac-Kan carrying a genome fragment resulting in a site-directed point mutation in *pilA* (resulting in PilA[T72C]); Kan^R	MB#8959	This study
pGP704-Sac-Kan-pilA[T75C]	pGP704-Sac-Kan carrying a genome fragment resulting in a site-directed point mutation in *pilA* (resulting in PilA[T75C]); Kan^R	MB#8960	This study

Table 2. Statistics on PacBio genome sequencing data and assembly

	***A. baumannii* A118**
Internal strain ID	MB#5144
BioSample ID	SAMN15507634
BioSample submission ID	SUB7757178
GenBank accession number	CP059039
Number of bases	662,248,721 bp
Number of reads	39,350
Mean read length	16,829 bp
Total number of contigs	1
Maximum contig length	3,787,003 bp
Contig length after circularization	3'750'370 bp
Total genome size	3'750'370 bp
Mean coverage	163 x
GC content	39.1 %

Table 3. Competence and TFP-related genes in strain A118

Gene names*	Locus tags in A118# (H0N27_ XXXXX)	Automatically annotated gene products in A118#	Homologs$		
			V. cholerae N16961 (VC(A)XXXX)	*A. baylyi* ADP1 (ACIADXXXX)	*P. aeruginosa* PAO1 (PAXXX)
Type IV pilus					
pilM	01440	pilus assembly protein PilM	*pilM (2634)*	*pilM (3360)*	*pilM (5044)*
pilN	01445	PilN domain-containing protein	*pilN (2633)*	*pilN (3359)*	*pilN (5043)*
pilO	01450	type 4a pilus biogenesis protein PilO	*pilO (2632)*	*pilO (3357)*	*pilO (5042)*
pilP	01455	pilus assembly protein PilP	*pilP (2631)*	*pilP (3356)*	*pilP (5041)*
pilQ	01460	type IV pilus secretin PilQ family protein	*pilQ (2630)*	*pilQ (3355)*	*pilQ (5040)*
pilT	13360	type IV pilus twitching motility protein PilT	*pilT (0462)*	*pilT (0912)*	*pilT (0395)*
pilU	13365	PilT/PilU family type 4a pilus ATPase	*pilU (0463)*	*pilU(0911)*	*pilU (0396)*
pilF	14985	type IV pilus biogenesis/stability protein PilW	*pilF (1612)*	*pilF (0558)*	*pilF (3805)*
fimV	15350	hypothetical protein	-	-	*fimV (3115)*
pilA	01510	pilin	*pilA (2423)*	*comP (3338)*	*pilA (4525)*
pilB	15830	type IV-A pilus assembly ATPase PilB	*pilB (2424)*	*pilB (0362)*	*pilB (4526)*
pilC	15835	type II secretion system F family protein	*pilC (2425)*	*pilC (0361)*	*pilC (4527)*
pilD	15840	prepilin peptidase	*pilD (2426)*	*pilD (0360)*	*pilD (4528)*
tsaP	16565	LysM peptidoglycan-binding domain-containing protein	*tsaP (0047)*	*0210*	*0020*
fimU	01560	GspH/FimT family pseudopilin	*VC0858 (part of minor pilin cluster; Seitz and Blokesch 2013)*	*fimU (3321)*	*fimU (4550)*
pilV	01565	type IV pilus modification protein PilV	-	*pilV (3319)*	*pilV (4551)*
pilW	01570	PilW family protein	-	*comB (3318)*	*pilW (4552)*
pilX	01575	pilus assembly protein	-	*pilX (3317)*	-
pilY1	01580	VWA domain-containing protein	-	*comC (3316)*	*pilY1 (4554)*
gene name to be defined	01585	prepilin-type N-terminal cleavage/methylation domain-containing protein	-	*comE (3315)*	-
pilE	01590	prepilin-type N-terminal cleavage/methylation domain-containing protein	*VC0857 (part of minor pilin cluster; Seitz and Blokesch 2013)*	*comF (3314)*	*pilE (4556)*
fimT	02975	GspH/FimT family pseudopilin	-	*fimT (0695)*	*fimT (4549)*
DNA uptake & translocation					
comEA	14695	ComEA family DNA-binding protein	*comEA (1917)*	*comEA (3064)*	*3140*
comEC	04190	DNA internalization-related competence protein ComEC/Rec2	*comEC (1879)*	*comA(2639)*	*comEC (2984)*
comF	01930	ComF family protein	*comF (2719)*	*comF (3236)*	*comF (0489)*

ssDNA binding & recombination					
ssb	00985	single-stranded DNA-binding protein	*ssb (0397)*	*ssb (3449)*	*ssb (4232)*
dprA	16570	DNA-protecting protein DprA	*dprA (0048)*	*0309*	*0021*
recA	07425	recombinase RecA	*recA (0543)*	*recA (1385)*	*recA (3617)*
comM	16365	YifB family Mg chelatase-like AAA ATPase	*comM (0032)*	*0242*	*5290*
TFP regulation					
pilS	16280	PAS domain-containing sensor histidine kinase	-	*pilS (0259)*	*pilS (4546)*
pilR	16285	sigma-54-dependent Fis family transcriptional regulator	-	*pilR (0258)*	*pilR (4547)*
pilG	03110	twitching motility response regulator PilG	-	*pilG (0786)*	*pilG (0408)*
pilH	03115	response regulator	-	*pilH (0787)*	*pilH (0409)*
pilI	03120	purine-binding chemotaxis protein CheW	-	*pilI (0788)*	*pilI (0410)*
pilJ	03125	methyl-accepting chemotaxis protein	-	*pilJ (0789)*	*pilJ (0411)*
-	*non-existent*	???	-	-	*pilK (0412)*
chpA	03130	Hpt domain-containing protein	-	*chpA (0790)*	*chpA (0413)*
to be defined	03135	hypothetical protein (predicted as cheA-like protein by HHpred)	-	-	-
-	*non-existent*	???	-	-	*chpB (0414)*
-	*non-existent*	???	-	-	*chpC (0415)*
-	*non-existent*	???	-	-	*chpD (0416)*
-	*non-existent*	???	-	-	*chpE (0417)*
cyaB	09340	adenylate/guanylate cyclase domain-containing protein	-	*1397*	*cyaB (3217)*
to be defined	11735	cAMP-activated global transcriptional regulator CRP	*crp (2614)*	*vfr (1262)*	*vfr (0652)*
fimL	12210	chemotaxis protein	-	*1136*	*fimL (1822)*
other genes					
glmS	00430	glutamine-fructose-6-phosphate transaminase (isomerizing)	*remark: next to mTn7 insertion site*		
hcp	11090	type VI secretion system tube protein Hcp	*remark: aph* (Kan^R) cassette inserted in tDNA		

* A118 gene names are according to (81) and (60). The genetic organization of competence genes as single genes or operons is indicated with arrows.

[#] Locus tags of strain A118 and automatic annotations are according to accession number CP059039.

[$] Homologs were determined using PATRIC BLAST and are based on protein sequence similarities, the positions of genes in operons, and their predicted functions. Only significant BLAST hits are shown (E value < 0.01).

- Locus tags of strain N16961 (VC(A)XXXX) are according to accession numbers NC_002505 & NC_002506 (82).
- Locus tags of strain ADP1 (ACIADXXXX) are according to accession number NC_005966 (83).
- Locus tags of strain PAO1 (PAXXX) are according to accession number NC_002516 (84).

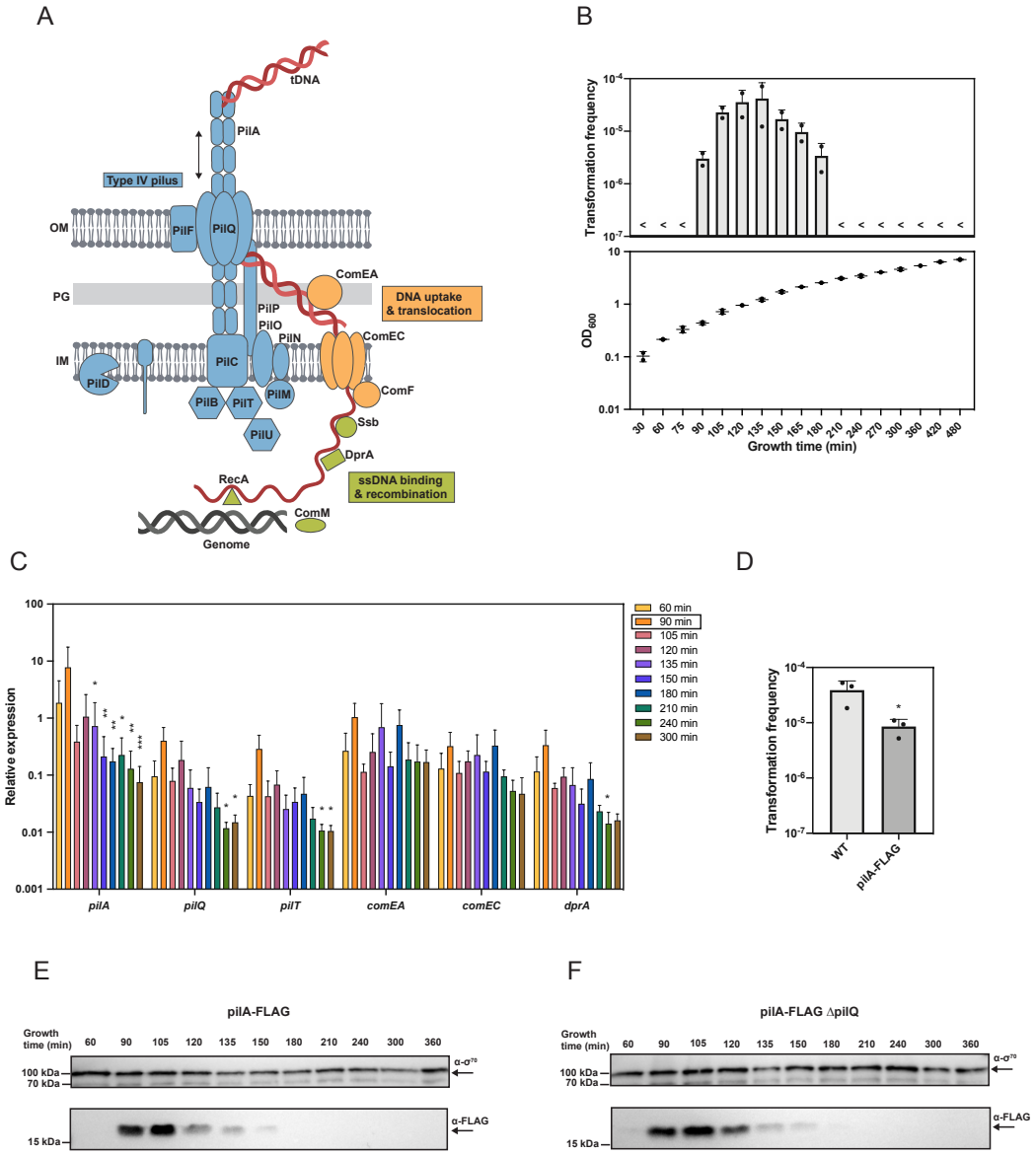

Figure 1. Transformation is growth-phase dependent in *A. baumannii*. A) Schematic representation of DNA uptake machinery. Type IV pilus (TFP) components shown in blue, DNA uptake and translocation proteins in orange, and proteins for binding and recombination of the incoming ssDNA in green. **B)** Natural transformability of *A. baumannii* over time. The graph on top shows the transformation frequencies, while the graph on the bottom depicts the growth of the bacteria given as in optical density at 600 nm (OD_{600}) units. **C)** Relative expression values over time for a subset of competence genes (*pilA*, *pilQ*, *pilT*, *comEA*, *comEC,* and *dprA*). **D)** Transformation frequencies of the wild-type (WT) and the strain encoding the PilA-FLAG translational fusion. **E-F)** Immunoblotting of FLAG-tagged PilA at different time points through the bacterial growth phases (as indicated in minutes) in the *pilA*-FLAG strain (D) or its *pilQ*-negative derivative (*pilA*-FLAGΔ*pilQ*) (E). Detection of Sigma70 served as loading control. Two and three biologically independent experiments were performed for panels (B) and (C-F), respectively, and the mean values (±SD) are shown for all graphs. <, below detection limit. Statistical analyses were performed on log-transformed data. Statistics was based on (C) a two-way ANOVA test with Tukey's multiple comparisons (time points compared to 90 min, as indicated by the box in the legend) or (D) an unpaired *t* test with Welch's correction. **P*<0.05, ***P*<0.01, ****P*<0.001.

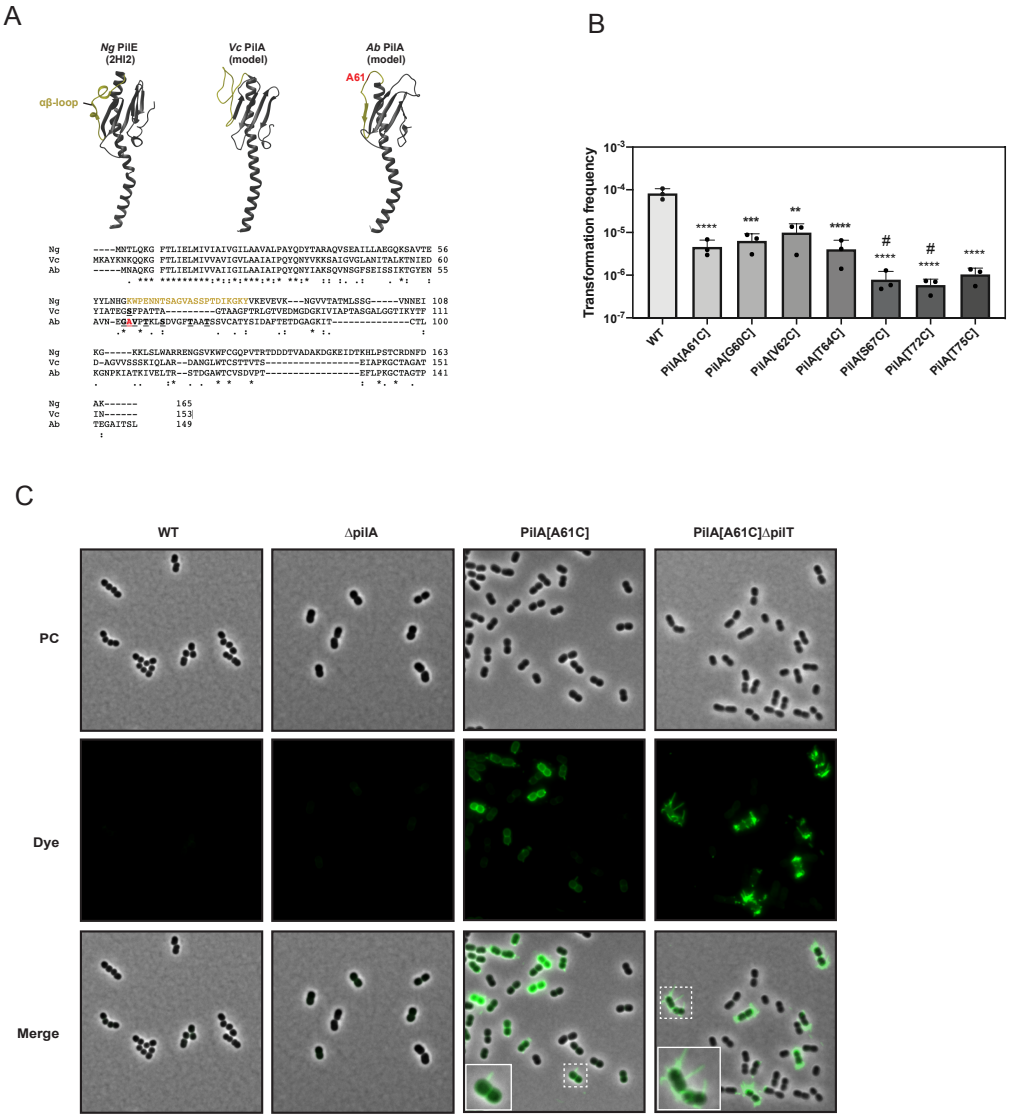

Figure 2. Design and functionality of PilA cysteine knock-in variants. A) 3D structural model of the *Neisseria gonorrhoeae* major type IV pilin PilE (PDB, 2HI2; (77)), which is shown alongside Phyre2 (50) structural predictions of the major pilin PilA of pandemic *V. cholerae* and of PilA of *A. baumannii* strain A118 (this study). The conserved αβ–loops are shown in greenish-yellow and the residue chosen for the cysteine exchange (A61) is shown in red. Bottom panel: Sequence alignments of *N. gonorrhoeae* PilE (Ng, Uniprot; P02974), *V. cholerae* PilA (Vc; protein ID AWB74893.1 (78)) and *A. baumannii* PilA (Ab; strain A118 & protein ID H0N27_01510) using Clustal Omega. The αβ–loop is coloured in yellow. The functional cysteine substitution in *V. cholerae'*s PilA is highlighted (S67; (22)). Residues tested in *A. baumannii* in this study are shown in bold and underlined. **B)** Natural transformability of PilA cysteine knock-in variants. Bars show the average transformation frequency of three independent experiments (±SD). Statistical analyses were performed on log-transformed data using a one-way ANOVA followed by Sidak's multiple comparisons test. Each mutant strain is compared to the WT strain. #, under detection limit in at least one experiment, in which case the detection limit was used for the calculation of the average value and statistical analyses. $^{**}P<0.01$, $^{***}P<0.001$, $^{****}P<0.0001$. **C)** Pilus imaging using a thiol-reactive maleimide dye. Snapshot images of A118-*pilA*[A61C] and A118-*pilA*[A61C]Δ*pilT* and the parental WT strain. The ΔpilA strain served as an additional negative control. The bacteria were stained with AF-488-Mal and imaged in the phase contrast (PC) or green fluorescence (Dye) channels. A merged image of both channels is shown in the bottom row (Merge). The contrast of the merged images was adjusted for best pilus visualization. An enlargement of the marked region (dotted boxes) is shown as an inset. Bar = 5 µm.

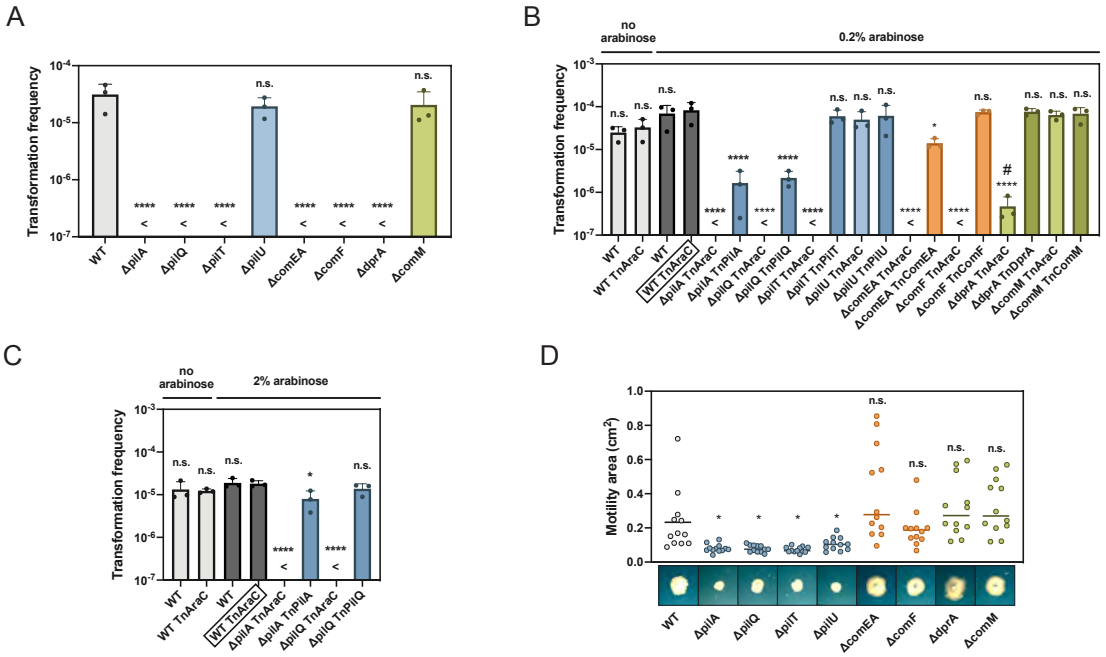

Figure 3. Type IV pilus genes are essential for transformation and surface motility. A-C) Transformation frequencies of defined mutants (details as in Fig. 1). For complementation, the strains carried a transposon without (control, TnAraC; no gene downstream of P_{BAD} promoter) or with (TnXXXX) the complementing gene on their chromosome and were grown in the absence or presence of 0.2% (B) or 2% (C) arabinose. For all bar plots, transformation frequencies of three independent experiments are plotted as mean values (±SD). <, below detection limit. #, under d.l. in at least one replicate (d.l. used for calculation of mean value). Log-transformed data was used for statistical analysis. When no transformants were obtained, the mean of the detection limit (d.l.) was used for statistical analyses. **D)** TFP mutants are non-motile on solid surfaces. Surface motility of the mutants described in panel A is depicted on the *Y*-axis based on the occupied area on the motility plates. Four biological experiments with three technical replicates are shown for each strain (n=12). Images from one experimental set are shown below the graph. Statistical analyses: (A-C) One-way ANOVA, using Sidak's multiple comparisons test; (D) Brown-Forsythe and Welch ANOVA tests with unpaired t with Welch's correction. *P<0.05, ****P<0.0001, n.s., not significant. The strains were compared to the WT (A, D) or the most appropriate control strain (boxed strain name in B and C).

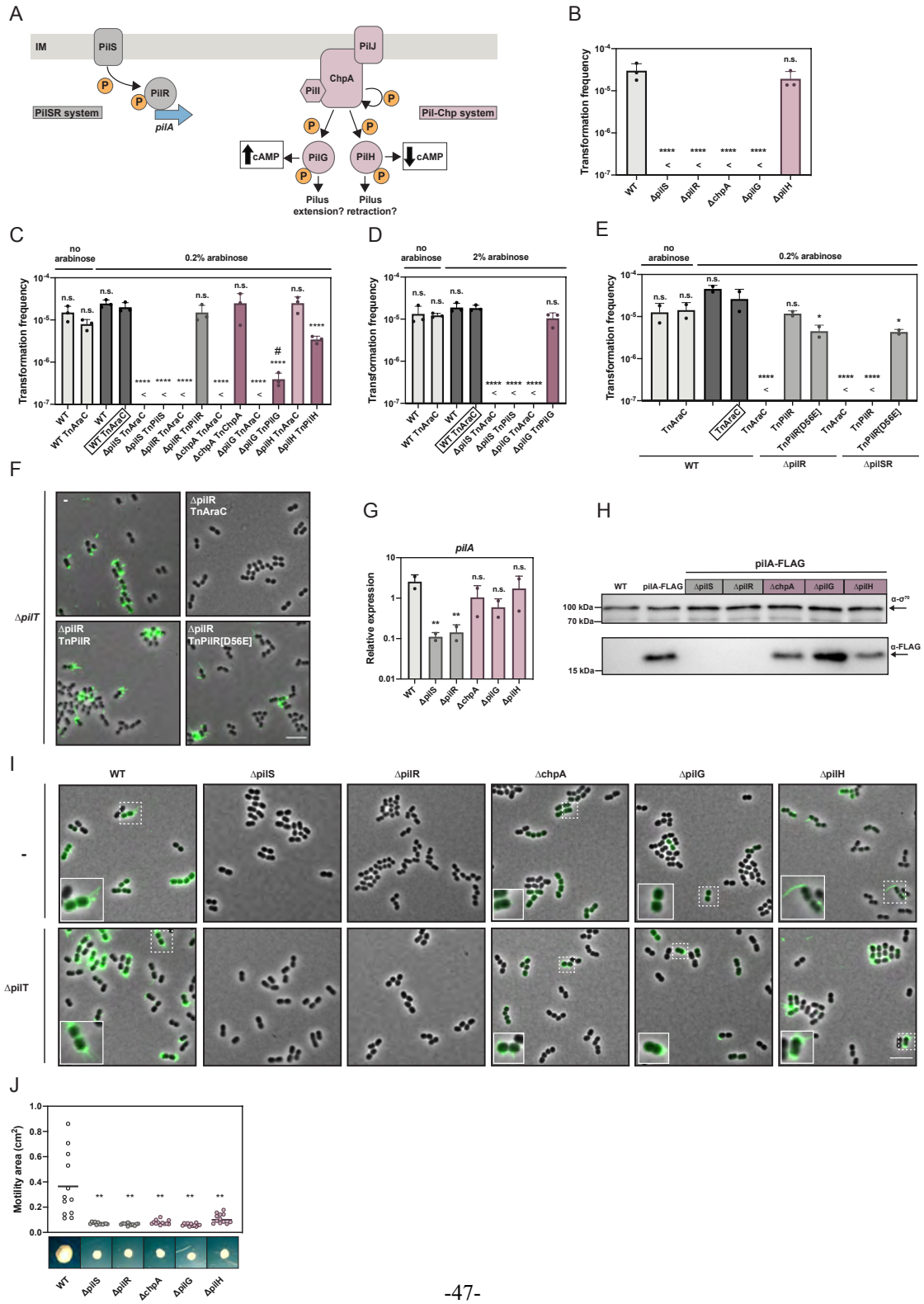

Figure 4. The *A. baumannii* PilSR and Pil-Chp systems are required for natural transformation and surface motility. **A)** Schematic representation of the PilSR and Pil-Chp systems. Left (gray): Upon activation, PilS phosphorylates PilR, which promotes expression of *pilA*. Right (purple): PilJ promotes auto-phosphorylation of ChpA, which subsequently phosphorylates PilG and/or PilH, resulting in increased or decreased cAMP levels, respectively. PilG and PilH were also proposed to foster T4P extension or retraction. **B-E)** Transformability of TFP regulation mutants without or with complementing constructs ± inducer, as indicated. Details as in Fig. 3. The WT and WT-TnAraC served as controls. Transformation frequencies are shown as mean value (±SD) of three independent experiments. <, below detection limit (d.l.). For statistical analyses, a one-way ANOVA with Sidak's multiple comparisons test was performed on log-transformed data and the different strains' values were compared to the WT (B) or to the most appropriate control strain (boxed name in C-E). #, under detection limit in at least one replicate. *P<0.05, ****P<0.0001, n.s. = not significant. **F + H)** Imaging of TFP in the regulatory mutants. PilA[A61C] pilus imaging of *pilT*-positive or *pilT*-negative strains (as indicated). For F) The strains were *pilR*-positive or *pilR*-negative and carried complementing *pilR* or its phosphomimetic *pilR*[D56E] variant on a transposon, as indicated. For H) The strains were deleted for the regulatory gene that is indicated above each column. Details as in Fig. 2, with the exception that only the merged images are shown. Bar = 5 µm (enlarged images are 2x magnified). **G)** Relative expression of *pilA* in the regulatory mutants. Average values (±SD) of two independent experiments are shown and statistics reflect a two-way ANOVA with Tukey's multiple comparisons test in which each strain was compared to the WT. **P<0.01, n.s. = not significant. **H)** Detection of PilA-FLAG in the different regulatory mutants. Representative images of two independent replicates. Details as in Fig. 1. **J)** TFP regulatory mutants are non-motile. The surface motility of the PilSR/ChpA system mutants is shown. Details as in Fig. 3D. The motility values of each strain were compared to the WT using Brown-Forsythe and Welch ANOVA tests with unpaired t with Welch's correction. **P<0.01.